PNNL-32851, Rev. 0
RPT-DFTP-032, Rev. 0

Fiscal Year 2022 Filtration of Hanford Tank 241-AP-101 Supernatant at 16 °C

June 2022

JR Allred
EC Buck
CA Burns
RC Daniel
JGH Geeting
ZB Webb
AM Westesen
RA Peterson

U.S. DEPARTMENT OF ENERGY

Prepared for the U.S. Department of Energy
under Contract DE-AC05-76RL01830

DISCLAIMER

This report was prepared as an account of work sponsored by an agency of the United States Government. Neither the United States Government nor any agency thereof, nor Battelle Memorial Institute, nor any of their employees, makes **any warranty, express or implied, or assumes any legal liability or responsibility for the accuracy, completeness, or usefulness of any information, apparatus, product, or process disclosed, or represents that its use would not infringe privately owned rights**. Reference herein to any specific commercial product, process, or service by trade name, trademark, manufacturer, or otherwise does not necessarily constitute or imply its endorsement, recommendation, or favoring by the United States Government or any agency thereof, or Battelle Memorial Institute. The views and opinions of authors expressed herein do not necessarily state or reflect those of the United States Government or any agency thereof.

PACIFIC NORTHWEST NATIONAL LABORATORY
operated by
BATTELLE
for the
UNITED STATES DEPARTMENT OF ENERGY
under Contract DE-AC05-76RL01830

Printed in the United States of America

Available to DOE and DOE contractors from the
Office of Scientific and Technical Information,
P.O. Box 62, Oak Ridge, TN 37831-0062;
ph: (865) 576-8401
fax: (865) 576-5728
email: reports@adonis.osti.gov

Available to the public from the National Technical Information Service
5301 Shawnee Rd., Alexandria, VA 22312
ph: (800) 553-NTIS (6847)
email: orders@ntis.gov <https://www.ntis.gov/about>
Online ordering: http://www.ntis.gov

Fiscal Year 2022 Filtration of Hanford Tank 241-AP-101 Supernatant at 16 °C

June 2022

JR Allred
EC Buck
CA Burns
RC Daniel
JGH Geeting
ZB Webb
AM Westesen
RA Peterson

Prepared for
the U.S. Department of Energy
under Contract DE-AC05-76RL01830

Pacific Northwest National Laboratory
Richland, Washington 99354

Summary

Bench-scale filtration testing of ~9 liters of supernatant from Hanford waste tank 241-AP-101, chilled to 16 °C, was conducted using a backpulse dead-end filter (BDEF) filtration system equipped with a feed vessel and a Mott inline filter Model 6610 (Media Grade 5) in the hot cells of the Radiochemical Processing Laboratory at Pacific Northwest National Laboratory. This was done to assess the performance of the anticipated third feed to the Tank Side Cesium Removal (TSCR) system. The as-received samples were diluted to the target sodium concentration and transferred to 1.5-liter polyethylene bottles and held at 16 °C for approximately 1 week prior to filtration. Similar to AP-105 and AP-107, no visible solids were observed in the as received or diluted samples.

The feed was filtered through the BDEF system at a targeted flux of 0.065 gpm/ft^2 to match the prototypic operation of the TSCR system. During filtration, the differential pressure required to effect filtration at 0.065 gpm/ft^2 increased little over the filtration campaign and never reached 2 psid (the TSCR action limit). This indicates that the TSCR filter should perform well when processing AP-101 supernatant. After completing filtration of the AP-101 feed, the filter was cleaned.

Solids concentrated from the backpulse solutions displayed sodium nitrate-type phases, aluminum and silicon phases reported as cancrinite or nitrate-cancrinite, a mixed chromium-aluminum oxide, iron oxides, and Ca-bearing phases (calcite). Scanning electron microscopy analyses showed that the average particle size was 0.5 micron. The amount of solids in the ~9 liters of supernatant tested did not have any measurable impact on filtration.

Acknowledgments

The authors gratefully acknowledge the help of hot cell technicians Victor Aguilar and Robert Cox in conducting this work. We thank Renee Russell for conducting the technical review of this report. We also thank Matt Wilburn for technical editing of this report and Bill Dey for the quality reviews of the calculation packages and this report.

Microscopy work was performed at the Radiochemical Processing Laboratory Quiet-Suite at Pacific Northwest National Laboratory.

Acronyms and Abbreviations

AEA	alpha energy analysis
AOI	analyte of interest
BDEF	backpulse dead-end filter (system)
BSE	backscattered electron
CWF	clean water flux
EDS	X-ray energy dispersive spectroscopy
EELS	electron energy loss spectroscopy
HAADF	high-angle annular dark-field
ICP-MS	inductively coupled plasma mass spectrometry
ICP-OES	inductively coupled plasma optical emission spectroscopy
IX	ion exchange
LAW	low-activity waste
MFC	mass flow controller
PLM	polarized light microscope
PNNL	Pacific Northwest National Laboratory
QA	quality assurance
R&D	research and development
RPL	Radiochemical Processing Laboratory
SAED	selected area electron diffration
SE	secondary electron
SEM	scanning electron microscopy
STEM	scanning transmission electron microscopy
TEM	transmission electron microscopy
TRU	transuranic
TSCR	Tank Side Cesium Removal
TWINS	Tank Waste Information Network System
WRPS	Washington River Protection Solutions
WTP	Waste Treatment and Immobilization Plant
WWFTP	WRPS Waste Form Testing Program

Contents

Summary ... iii
Acknowledgments ... iv
Acronyms and Abbreviations ... v
Contents ... vi
1.0 Introduction ... 1.1
2.0 Quality Assurance ... 2.1
3.0 Test Conditions ... 3.1
  3.1 BDEF Filtration ... 3.1
    3.1.1 Backpulse Dead-End Filter (BDEF) System Description ... 3.1
    3.1.2 System Operation during Testing ... 3.3
  3.2 Dilution ... 3.4
  3.3 Feed Temperature Control ... 3.5
  3.4 Sample Analysis ... 3.8
4.0 Results ... 4.1
  4.1 Dilution Process Results ... 4.1
  4.2 Clean Water Flux ... 4.1
  4.3 Waste Filtering ... 4.2
  4.4 Final CWF ... 4.7
  4.5 Analytical Results ... 4.7
    4.5.1 River Water Analysis ... 4.7
    4.5.2 As-Received AP-101 Supernate Tank Waste Analysis ... 4.8
    4.5.3 Total Alpha Energy Analysis ... 4.9
    4.5.4 Rheology Analysis of Filtered and Cesium Decontaminated AP-101 Supernate Tank Waste ... 4.9
  4.6 Microscopy Solids Analysis ... 4.10
5.0 Conclusions ... 5.1
6.0 References ... 6.1
Appendix A – BDEF Piping and Instrumentation Diagram ... A.1
Appendix B – Total Alpha Analysis for Filtration Permeate Samples ... B.1
Appendix C – ICP-OES Analysis for Raw Columbia River Water ... C.1
Appendix D – ICP-OES Analysis for As-Received 241-AP-101 Supernatant ... D.1
Appendix E – Backpulse AP-101 Characterization with Scanning Electron Microscopy Coupled with Automated Particle Analysis ... E.1

Figures

Figure 3.1. BDEF system installed in hot cell. HTX = heat exchanger. 3.2
Figure 3.2. (a) Filter housing schematic (note that the 6610 series filter was welded to a 3/8-in. pipe fitting, making the configuration similar to the 6480 series illustrated here); (b) photo of modified filters with filter housings removed. 3.3
Figure 3.3. AP-101 temperature in the trough heat exchanger. 3.6
Figure 3.4. AP-101 temperature in the BDEF recirculation loop. 3.7
Figure 3.5. AP-101 temperature in the clamshell heat exchanger. 3.7
Figure 3.6. Concentrated solids after centrifuging. 3.8
Figure 3.7. Concentrated solids after rinse and air drying. 3.9
Figure 4.1. CWF measurements for Media Grade 5 BDEF at 2.57 milliliter/minute (0.065 gpm/ft^2) permeate rate (nominal) before testing. (Dashed line is average pressure over the 10-minute period.) 4.2
Figure 4.2. AP-101 density during filtration process. 4.5
Figure 4.3. Filter differential pressure and MFC flow rate during waste filtering operations. 4.6
Figure 4.4. Initial and final clean water flux. 4.7
Figure 4.5. SEM images of example morphologies observed from the filtered AP-101 supernatant: (A) distribution of particles taken at low magnification, (B) high surface area agglomerate. 4.10
Figure 4.6. Backscatter electron (BSE) images and elemental maps of a particle agglomerate from AP-101 supernatant-solids. The elemental maps show the presence of a round aluminosilicate phase (indicated by arrow). 4.11
Figure 4.7. Effect of dissolution on the particle composition of AP-101 supernatant through ternary phase diagrams and compositional-particle size distributions, showing the loss of sodium bearing phases. 4.11

Tables

Table 3.1. Mass balance – BDEF. 3.4
Table 4.2. System timeline. 4.3
Table 4.3. Post filtration density measurements of product bottles. 4.6
Table 4.4. ICP-OES analyte concentration in river water (ASR 1393). 4.8
Table 4.5. ICP-OES and ICP-MS results of as-received AP-101 supernate tank waste. 4.9
Table 4.6. AEA for permeate samples. 4.9
Table 4.7. Viscosity results of filtered and Cs decontaminated sample. 4.10

1.0 Introduction

The U.S. Department of Energy's Hanford Site houses 56 million gallons of high-level radioactive waste generated from plutonium production from 1944 to 1988 (Gerber 1992). The supernatant waste, currently stored in underground tanks, is intended to be vitrified following filtration and ^{137}Cs removal at the Hanford Waste Treatment and Immobilization Plant (WTP) Pretreatment Facility. Because the Pretreatment Facility will not be operational for several years, ^{137}Cs will be removed from low-activity waste (LAW) vitrification feeds using the Tank Side Cesium Removal (TSCR) system in a technology demonstration that will filter and then remove cesium from tank waste supernate to support transferring the TSCR-processed waste directly to the WTP LAW Melter Facility. The TSCR system is skid-mounted and employs two key technologies: (1) dead-end filtration for solids removal, which is necessary to protect the functionality of the ion exchange (IX) columns, and (2) IX for cesium removal.

A small-scale test platform was established in 2017 to demonstrate these processes in the Pacific Northwest National Laboratory (PNNL) 325 Building, also known as the Radiochemical Processing Laboratory (RPL).

Hanford waste tank 241-AP-101, from here called AP-101, is anticipated to be the third feed to TSCR, and thus was next in line for assessment after completion of testing with Hanford wastes from tanks 241-AP-107 and 241-AP-105 (referred to herein as AP-107 and AP-105). The purpose of this filtration testing was to (a) demonstrate dead-end filtration testing of AP-101 feed at 16 °C to obtain TSCR prototypic flux rates and identify issues that may impact filtration, and (b) provide feed to IX (also part of the test platform).

The presence of solids has been observed in previous filtration experiments using supernatant waste from AP-105 and AP-107 (Geeting et al. 2018a,b, 2019; Allred et al. 2020, 2021). Formation of solids in these tests was suspected to be due to tank mixing, dilution with process water, and reducing the feed temperature to 16 °C.

Therefore, the objective of the current work was to perform filtration under prototypic conditions using Mott Grade 5 sintered metal at the targeted flux of 0.065 gpm/ft^2 planned for TSCR, and at the lower (more challenging) TSCR operation temperature expected during the colder season. Filter resistance as a function of time was measured and the filter was backpulsed at the end of filtration testing. Backpulse solutions were collected and the solids were concentrated and assessed by microscopy methods.

2.0 Quality Assurance

All research and development (R&D) work at PNNL is performed in accordance with PNNL's Laboratory-Level Quality Management Program, which is based on a graded application of NQA-1-2000, *Quality Assurance Requirements for Nuclear Facility Applications* (ASME 2000), to R&D activities. To ensure that all client quality assurance (QA) expectations were addressed, the QA controls of PNNL's Washington River Protection Solutions (WRPS) Waste Form Testing Program (WWFTP) QA program were also implemented for this work. The WWFTP QA program implements the requirements of NQA-1-2008, *Quality Assurance Requirements for Nuclear Facility Applications* (ASME 2008), and NQA-1a-2009*, Addenda to ASME NQA-1-2008* (ASME 2009), and consists of the WWFTP Quality Assurance Plan (QA-WWFTP-001) and associated QA-NSLW-numbered procedures that provide detailed instructions for implementing NQA-1 requirements for R&D work.

The work described in this report was assigned the technology level "Applied Research" and was planned, performed, documented, and reported in accordance with procedure QA-NSLW-1102, *Scientific Investigation for Applied Research*. All staff members contributing to the work received proper technical and QA training prior to performing quality-affecting work.

3.0 Test Conditions

In October 2021, WRPS collected 36 supernatant samples (~250 mL) from tank 241-AP-101 in two batches (approximately 18 feet below the liquid surface level) and provided them to PNNL for filtration testing. At the RPL, PNNL diluted both batches with process water (Columbia River water) from approximately 8.5 M sodium (nominal tank concentration) to 5.5 M sodium in 1.5-liter polyethylene bottles, resulting in approximately 13.7 L of diluted tank waste. No visible solids were observed in the as received or diluted samples. The diluted AP-101 tank waste bottles were chilled (16 °C setpoint) for approximately 1 week prior to testing. Filtration testing of the tank waste using a Mott Model 6610 (Media Grade 5) line filter with porous end cap began on November 14, 2021. This is a sintered 316L stainless steel filter with a 0.317-in. porous diameter, 1.463-in. porous length, and 1.51-in.^{2} filter area.

3.1 BDEF Filtration

3.1.1 Backpulse Dead-End Filter (BDEF) System Description

The filtration system is the same system that was used in fiscal year 2020 (Allred et al. 2020), with a few modifications to support reduced-temperature filtration. Modifications included two additional heat exchangers installed in the hot cell (connected to two chillers) to control the temperature of the feed before and during filtration. The first new heat exchanger (trough heat exchanger) kept all the feed at the setpoint temperature until it was added to the BDEF system. The trough heat exchanger has dimensions of 9 in. × 25 in. × 12 in. (width, length, height) and a removable cover on the top. The feed bottles were stored in the trough heat exchanger with a cover until the feed was transferred to the BDEF system.

Once the feed was added to the BDEF, the existing heat exchanger kept the feed at the setpoint temperature in the reservoir and in the BDEF recirculation loop. The second new heat exchanger (clamshell heat exchanger) completely enclosed the filter and associated tubing to keep the feed at the setpoint temperature as it exited the recirculation loop until it was filtered. After filtration, the temperature was no longer controlled. A piping and instrumentation diagram is provided in Appendix A. A photograph of the BDEF system installed in the RPL Shielded Analytical Laboratory hot cell is shown in Figure 3.1.

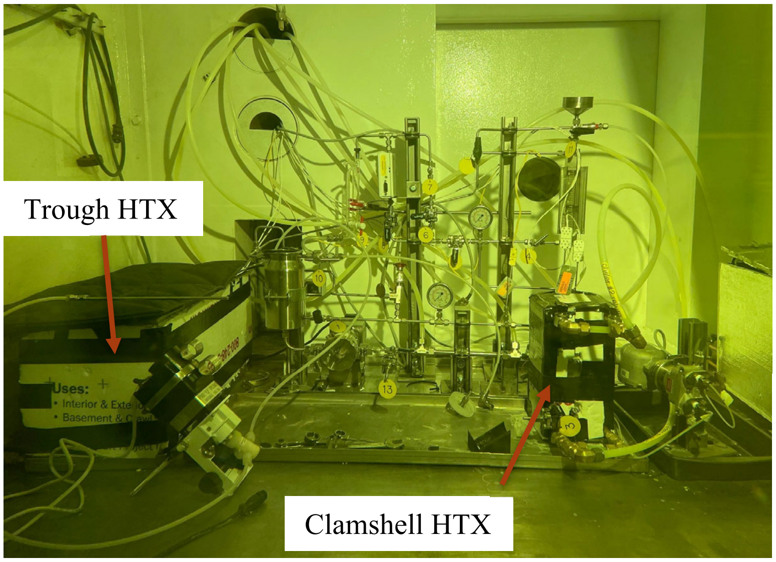

Figure 3.1. BDEF system installed in hot cell. HTX = heat exchanger.

The BDEF system is composed of a slurry recirculation loop, a filter assembly, and a permeate system. The main recirculation loop consists of a 1-liter stainless steel container (Eagle, EPV1A), a low-shear quaternary diaphragm pump (Quattro Flow QF150), a heat exchanger, and a throttle valve. The pump speed is controlled by a variable frequency drive that is located outside the hot cell. The slurry flow rate and pressure are controlled by adjusting the pump variable frequency drive (pump speed control) and throttle valve. The recirculation loop provides mixed, pressurized feed to the filter assembly. During the testing described in this report, the slurry temperature was controlled at a 16 °C setpoint.

The filter assembly receives pressurized slurry from the slurry recirculation loop. The filter assembly is composed of a filter, a Rosemount differential pressure transducer, and a flush valve (V3 in Appendix A). The flush valve is actuated during backpulse operations used to clear solids off the filter and out of the system.

The permeate system receives permeate produced by the filter assembly. The permeate flow rate is controlled with a mass flow controller (MFC), which can control feed in the range of 0.15 to 0.33 liter/hour. (These rates equate to allowable filter areas of 1.5 to 3.3 in.^{2} assuming flux of 0.065 gpm/ft^2.) The MFC measures flow rate and density of the permeate while a glass flowmeter is provided as a secondary flow rate measurement device. The permeate system can also perform a backpulse function. Pressurized air can be introduced (V12) into the backpulse chamber and used to force permeate (or other fluids) backward through the filter and out of the system through V3.

The Mott 6610 filter used in testing is cylindrical, with dimensions of 0.317-in. diameter × 1.5-in. length and a filtration area of 1.51 in.^{2}. The filter element is fabricated from a seamless sintered stainless-steel tube that is a closed/dead-end porous tube (with a porous end cap); the open end is welded to a pipe-reducing bushing. At 0.065 gpm/ft^2, the rate of filter processing is 3.7 L feed per 24-hour day. Figure 3.2 shows a schematic of the filter assembly and a photo of the filter.

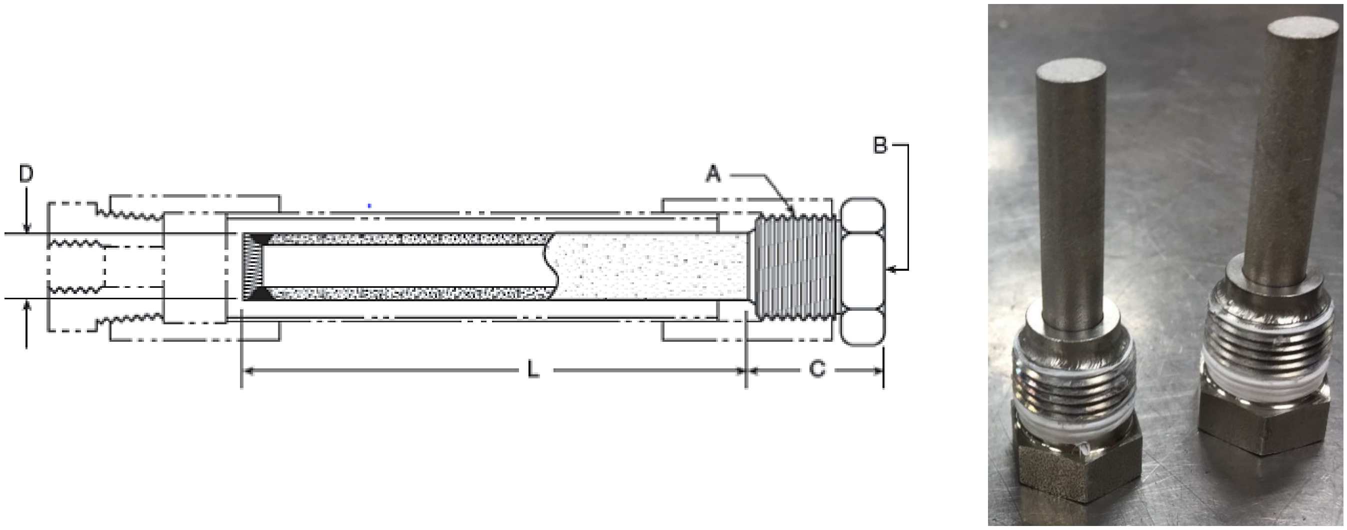

(a) (b)

Figure 3.2. (a) Filter housing schematic[1] (note that the 6610 series filter was welded to a 3/8-in. pipe fitting, making the configuration similar to the 6480 series illustrated here); (b) photo of modified filters with filter housings removed.

3.1.2 System Operation during Testing

The evolutions used to test the AP-101 waste samples are outlined below.

1. Dilute AP-101 feed from 8.5 M to 5.5 M sodium using process water. This activity was performed approximately 1 month prior to filtration.

2. Chill feed to 16 ± 2.2 °C for 1 week prior to the start of filtration.

3. Clean water flux (CWF) measurement: The CWF measurement served as a system leak test and provided a baseline measurement of the filter resistance and was conducted at nominal test conditions of 0.065 gpm/ft^2 and run for approximately 10 minutes.

4. Filter AP-101 with BDEF: Filter AP-101 feed with the BDEF at 0.154 liter/hour (0.065 gpm/ft^2). The targeted filtration rate was based on prototypic flux planned for TSCR. The filtration rate for BDEF testing was controlled with an MFC. Permeate was sampled after approximately 1/3, 2/3, and 3/3 (near the end) of the feed had been filtered.

   Filtration would continue until the differential pressure across the filter reached 2 psi, at which point the BDEF would have been backflushed. Backflush concentrate would be set aside for slurry sample analysis. Based on 13.7 liters of diluted feed, filtration should have lasted about 90 hours.

---

[1] Mott 6480 line filter from https://mottcorp.com.

5. Filter cleaning: If needed filter would have been periodically cleaned by draining the AP-101 feed and adding 0.1 M NaOH to the BDEF. (The drained feed would be maintained at the target temperature, 16 °C.) The hydroxide solution would be recirculated through the filter. The recirculation pump would be turned off and the filter soaked in the hydroxide solution for 2 hours. After the soak, the filter would be backpulsed and the system drained of the cleaning solution and then rinsed with 0.01 M NaOH solution.

   If needed the filter would have been cleaned after 24 hours or when 3 backpulses had been performed within a 24-hour period. If there had been no backpulses in a 24-hour period, filter cleaning would be deferred until 1 backpulse event had been triggered (differential pressure across the filter reaches 2 psi) or entire feed filtered. During the cleaning, the feed would be drained from the BDEF and stored in the trough chiller at 16 °C. Feed drained from the BDEF would be segregated and filtered last.

   Note: Evolutions 4 and 5 would have continued until all of the feed has been filtered. The BDEF filter would then be backflushed and cleaned at the conclusion of filtration.

6. CWF: After cleaning, the BDEF was rinsed and another CWF test was executed on the filter.

7. The BDEF system was laid-up for storage.

Table 3.1 provides a mass balance for the BDEF testing. A total of 16,226.1 g of AP-101 supernatant was added to the BDEF system during testing, and a total of 16,175.8 g was removed. The missing mass (~50 g) is likely due to evaporation and material that wets the inside of the BDEF system, is not recoverable, and represents less than 0.5% of the initial feed.

Table 3.1. Mass balance – BDEF.

Description	In (g)	Out (g)
Decanted supernate filtration	16,226.1	
Product to IX		16,028.2
Permeate samples		21.7
Backpulse samples		79.6
Drained from BDEF		46.3
Total	16,226.1	16,175.8

3.2 Dilution

Dilution of the feed material received from tank AP-101 was based on the Best Basis Inventory supernatant density from the Tank Waste Information Network System (TWINS) database[1] (accessed Oct 25, 2021). This value was 1.40 g/mL. Sodium concentration was also based on TWINS data and was assumed to be 8.595 M. The target end point Na concentration is 5.5 M with a density of 1.250 g/mL. Dilution was performed using raw (unprocessed) water from the Colombia River. The mass of raw water needed to be added (m_{add}) was estimated by

---

[1] The Best Basis Inventory is reported on the TWINS web site (http://twins.hanford.gov). To obtain the Best Basis Inventory, go to the web site and from its main menu select “Best Basis Inventory,” then “Best Basis Calculation Detail”.

$$m_{add} = \left(\frac{c_o\,\rho_1}{c_1\,\rho_o} - 1\right) m_o$$

where m_o is the mass of the undiluted tank waste; c_o and c_1 are the undiluted and diluted target Na concentrations, respectively; and ρ_o and ρ_1 are the undiluted and diluted simulant densities, respectively. The dilution factor is defined as

$$DF = \frac{V_{final}}{V_{initial}}$$

where $V_{initial}$ is the initial solution volume and V_{final} is the final solution volume.

The contents of three AP-101 sample jars were combined and diluted with the process water at a mass ratio of nominally 1000:395 (undiluted tank waste: raw water) to achieve a volume dilution factor of 1.55:

$$\frac{m_{add}}{m_o} = \left(\frac{8.595\text{ M}}{5.50\text{ M}}\right)\left(\frac{1.250\text{ g mL}^{-1}}{1.40\text{ g mL}^{-1}}\right) - 1 = 0.395$$

3.3 Feed Temperature Control

Figure 3.3 provides the temperature profile of the AP-101 feed as it awaited introduction into the BDEF system for filtration. The feed was chilled and held at the 16 °C setpoint temperature for approximately 1 week before the start of filtration testing, beginning on 11/4/2021, and continued to be chilled throughout the filtration process. A 100-ohm platinum resistance temperature detector probe, labeled TE-104, measured the temperature in a feed bottle held in the trough heat exchanger and averaged 16.3 °C throughout the chilling duration. TE-104 was placed in feed bottles using a lid with a feedthrough, allowing TE-104 to be submerged without risk of spill.

Toward the end of the filtration operations at 0626 on 11/17/21, TE-104 needed to be repositioned and inserted into the lid used to feed the BDEF, due to minimal amount of supernatant liquid remaining. During this operation, the TE-104 probe was removed from the feed bottle for approximately 8 minutes, and a temporary spike in temperature is observed. The temperature reported by TI-104 returned to normal ranges upon the return of TE-104 to the feed bottle.

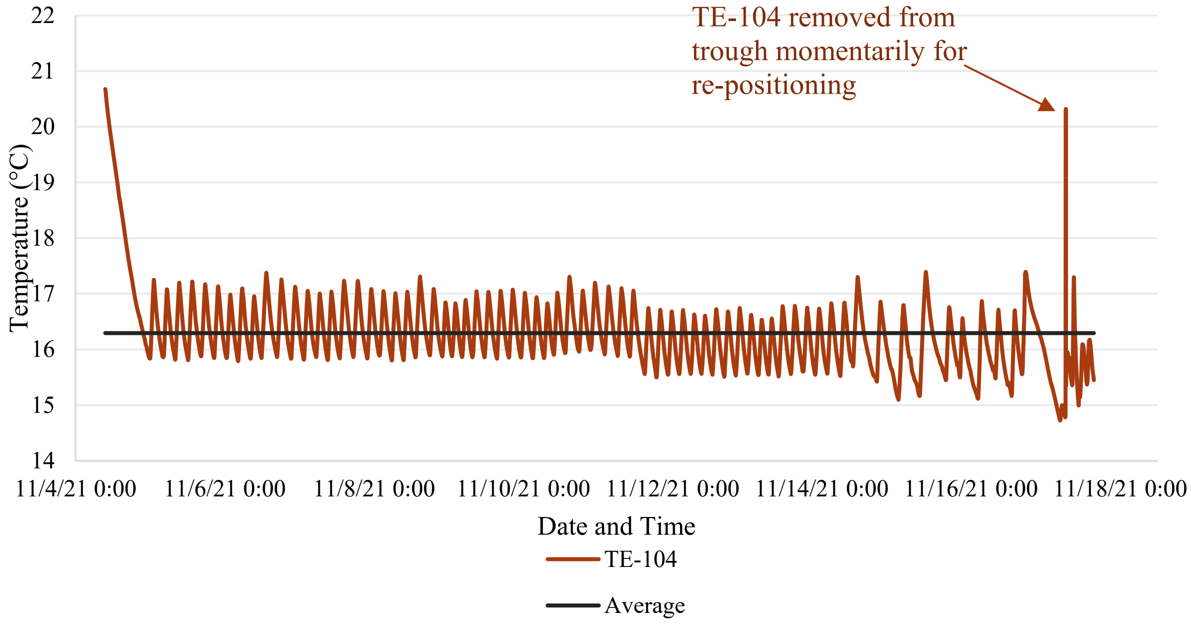

Figure 3.3. AP-101 temperature in the trough heat exchanger.

Figure 3.4 shows the temperature of the AP-101 in the BDEF recirculation loop (TE-101) during the entire filtration test. Similarly, the temperature profile of the AP-101 feed immediately before (TE-102) and after (TE-103) the filter, in the clamshell heat exchanger, is shown in Figure 3.5. Filtration of AP-101 started at 0924 on 11/11/2021 and concluded at 2136 on 11/17/2021. There was an initial drop in temperature at the outlet of the clamshell heat exchanger (TE-103) to 13.6 °C due to the chiller overcompensating for the beginning higher temperatures; however, the 16 °C setpoint was reached after approximately 2 hours of filtration. The lack of pressure build-up during the testing allowed all of the AP-101 feed to be filtered without any backpulsing or filter cleaning, keeping the tank waste within the 16 ± 1 °C range after the initial setpoint was reached.

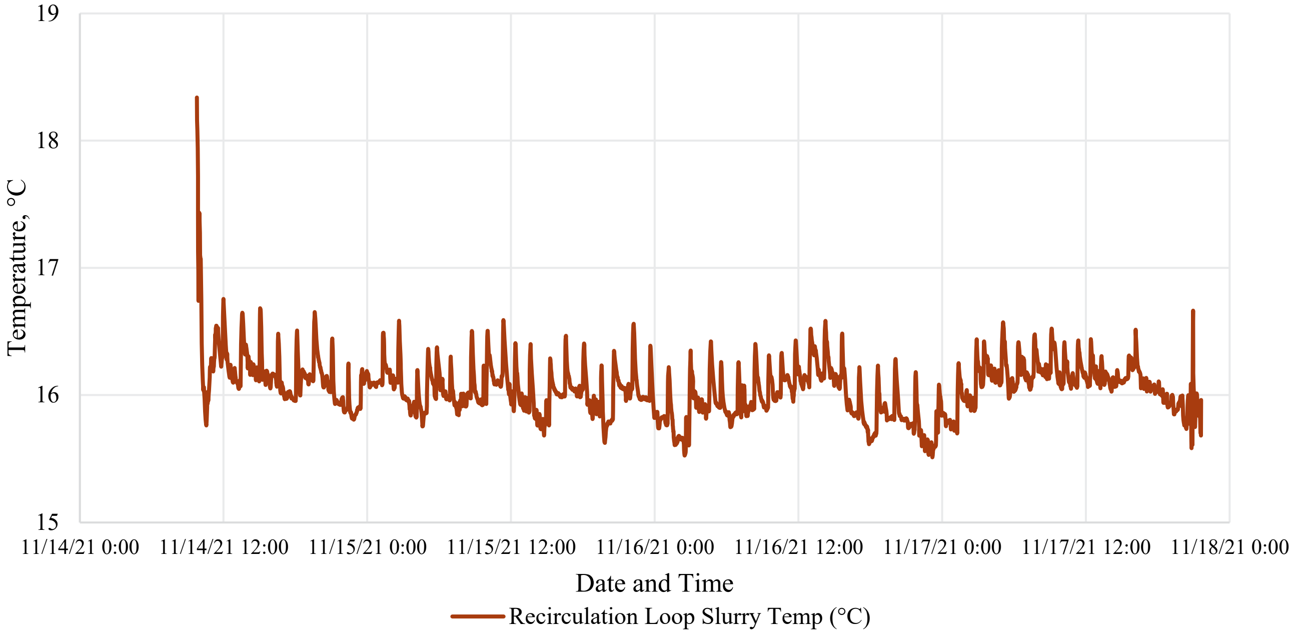

Figure 3.4. AP-101 temperature in the BDEF recirculation loop.

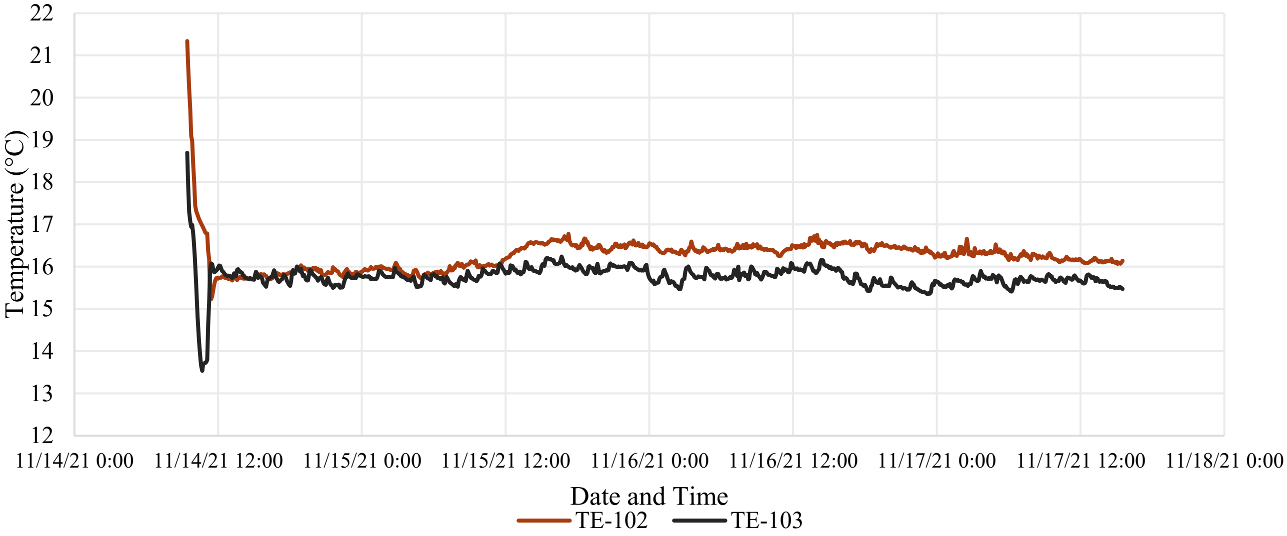

Figure 3.5. AP-101 temperature in the clamshell heat exchanger.

3.4 Sample Analysis

The process water (river water) used for dilution was analyzed via inductively coupled plasma optical emission spectroscopy (ICP-OES) for the following analytes of interest (AOIs): Ba, Ca, K, Mg, Na, S, Si, and Zn. The AP-101 tank waste supernate was analyzed as-received by ICP-OES and inductively coupled plasma mass spectrometry (ICP-MS) for the following AOIs: Al, K, Na, and Tc.

Three permeate samples (TI-125-P1, TI-125-P2, TI-125-P3) were collected after approximately 1/3, 2/3, and 3/3 of the AP-101 feed had been filtered. These samples were submitted for total alpha analysis to determine the transuranic (TRU) content of the filtered permeate.

One backpulse was performed following the filtration operations when the system was filled with AP-101 feed. To concentrate solids, solution collected from the feed backpulse event was centrifuged at 2500 rpm for 10 minutes. The bulk amount of the supernatant was decanted and the solids from the centrifuge tubes were suspended and combined. The consolidated solids were then split evenly into two separate samples, labeled TI-125-Solids-1 and TI-125-Solids-2. Each sample was decanted again and rinsed with 1.0 M NaOH/4.6M $NaNO_3$ solution. The rinsed solids were then centrifuged at 3000 rpm for 2 minutes. This process was performed two times. TI-125-Solids-1 was left to air dry for approximately 1 week, while TI-125-Solids-2 was left in approximately 1 mL of the 1.0 M NaOH/4.6M $NaNO_3$ solution. Very few solids were collected and there was only sufficient sample available to conduct scanning electron microscopy (SEM) analysis. The SEM results are reported in Section 4.6. Figure 3.6 shows the solids that were collected from the backpulsed solution after the solutions were centrifuged, and decanted. Figure 3.7 shows the solids after the 1.0 M NaOH/4.6M $NaNO_3$ rinsing process and air drying.

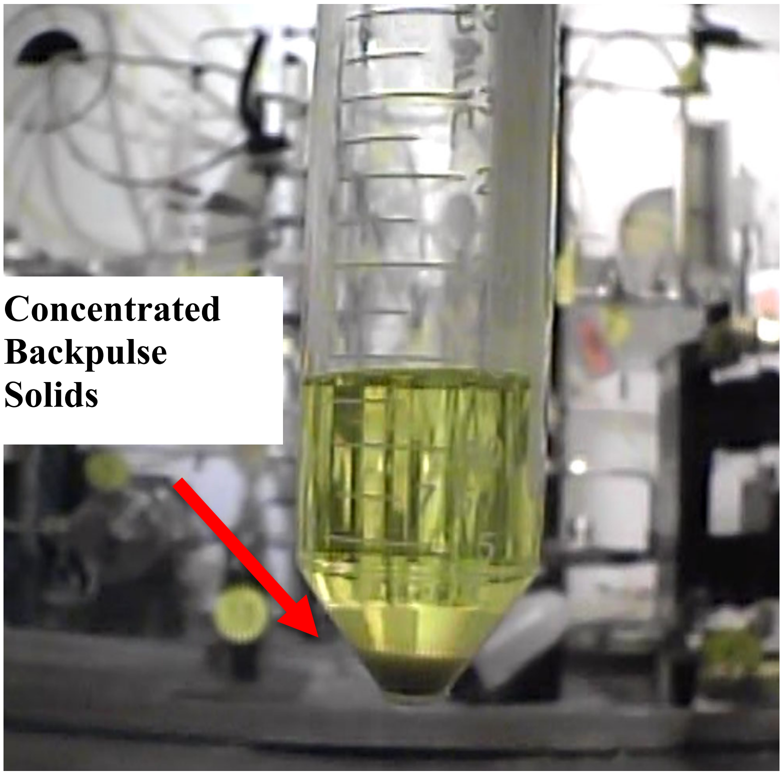

Figure 3.6. Concentrated solids after centrifuging.

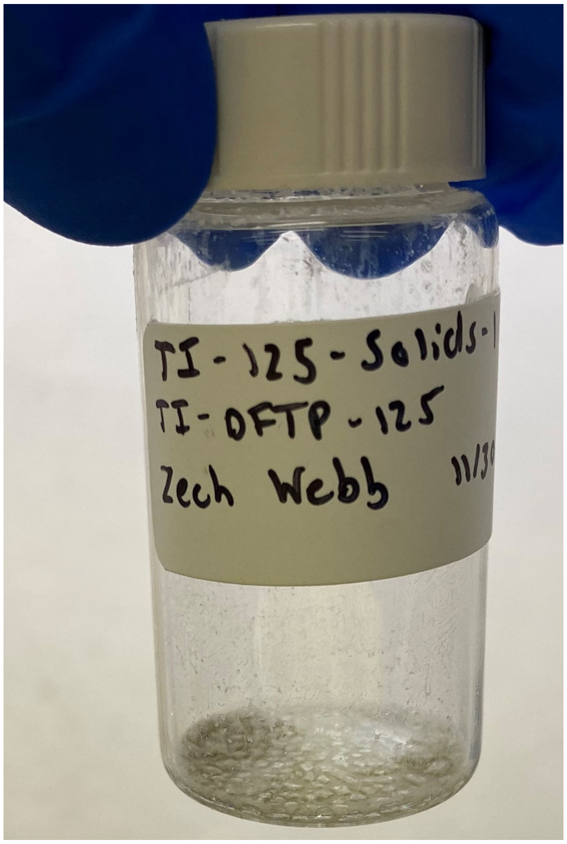

Figure 3.7. Concentrated solids after rinse and air drying.

4.0 Results

4.1 Dilution Process Results

A sample of the diluted AP-101 solution was checked for density to assess the dilution. Density measured via a 10-mL Class A volumetric flask and an analytical balance was recorded at 1.259 g/mL at an ambient cell temperature of 25.2 °C. The Na concentration was not measured after dilution but was measured after filtration (which should not affect Na concentration) and will be reported in the IX report for fiscal year 2022 (RPT-DFTP-034, *Reduced Temperature Cesium Removal from AP-101 Using Crystalline Silicotitanate*; currently being drafted).

The density of the raw water used for dilution was measured to be 0.99487 g/mL at 20.6 °C. Additional analysis of the raw water is detailed in Section 4.5.1.

4.2 Clean Water Flux

The objective of the CWF is to assess the state of the system at the start of testing to ensure a uniform basis for comparing different filtration trials, and in particular to ensure that the system is "clean" at the start of testing. Figure 4.1 shows the initial CWF at 16 °C using 0.01 M NaOH with the Media Grade 5 stainless steel BDEF filter. The CWF tests were conducted at ambient cell temperature at a nominal 2.57 mL/min (0.065 gpm/ft^2) permeate flow rate. The transmembrane pressure averaged 0.116 psid in the initial CWF with an average filter resistance of 1.65×10^{10} m^{-1}. Resistance, R [m^{-1}], is calculated via Darcy's law:

$$Q = \frac{PA_t}{\mu R}$$

where Q is the volumetric flow rate [m^3/s], P is the transmembrane pressure [Pa], A_t is the total filter area [m^2] [9.74×10^{-4} m^2], and μ is the filtrate dynamic viscosity [Pa·s] (assumed to be 1.11 cP @ 16 °C). Rearranging so that:

$$R(t) = \frac{P(t)A_t}{\mu Q(t)}$$

Prior CWF results on the BDEF system with this filter ranged from 0.015 to 0.1 psid transmembrane pressure (Allred et al. 2020). These values all are likely within the accuracy of the CWF measurement and represent a relatively clean filter. Estimates of the resistance for the Mott 6610 series Grade 5 are on the order of 2×10^{10} m^{-1}. By this metric, the filter is cleaner than the baseline flux. The downward curvature of the differential pressure during the CWF displays lack of fouling on the filter (due to residual solids in the system). As such, these results indicate an overall clean system at the start of testing.

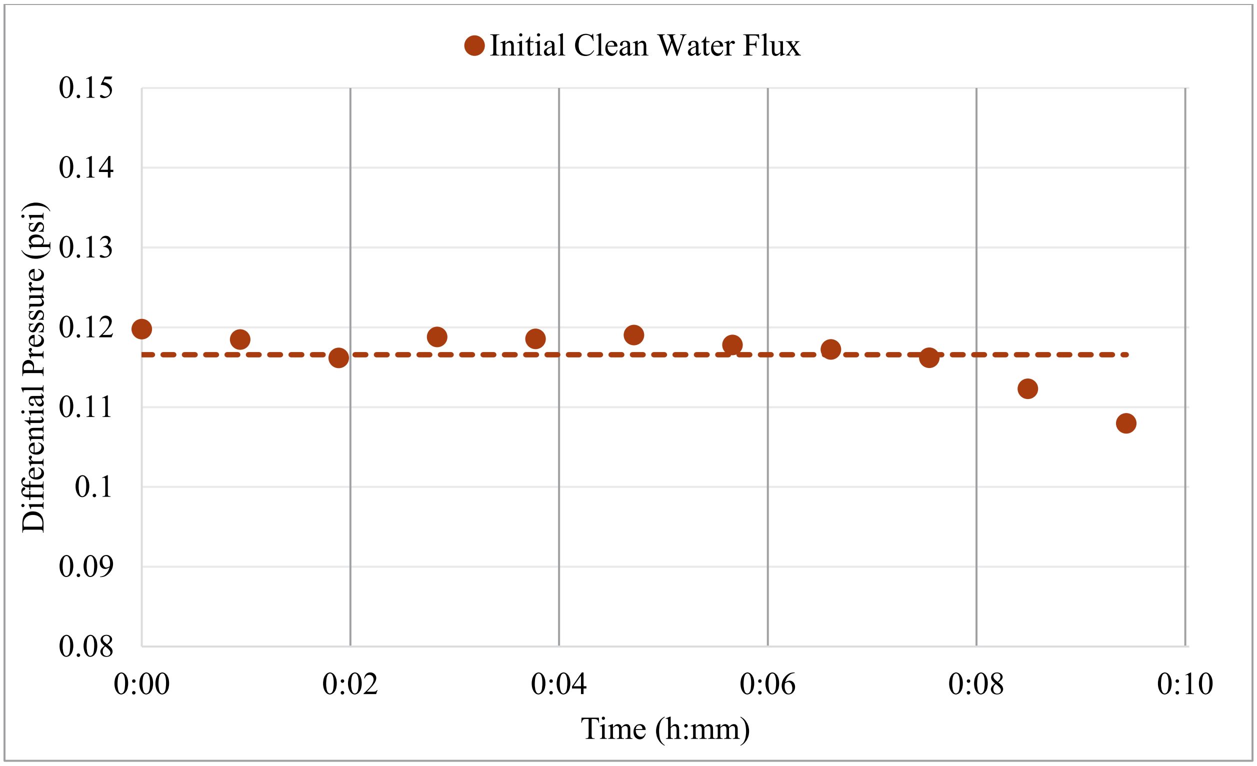

Figure 4.1. CWF measurements for Media Grade 5 BDEF at 2.57 milliliter/minute (0.065 gpm/ft^2) permeate rate (nominal) before testing. (Dashed line is average pressure over the 10-minute period.)

4.3 Waste Filtering

Each BDEF feed bottle was positioned in the trough heat exchanger to maintain feed temperature control (16 ± 1 °C). Feed was then transferred into the BDEF reservoir via metering pump until approximately 2 inches of AP-101 solution remained in the feed bottle. The remaining “bottoms” from each feed bottle were consolidated and fed into the system toward the end of the filtration process. The filtration rate was controlled via an MFC set at 2.57 mL/min (0.065 gpm/ft^2). The actual flow rate averaged 2.56 mL/min. Slurry recirculation line pressure was kept between 20 and 25 psi, with adjustments made for any deviations. No backpulses were performed during the filtration process. The transmembrane pressure did not reach the 2-psid limit (the threshold to indicate that a backpulse was needed) and averaged 0.21 psid throughout the testing.

Table 4.1 provides a timeline for the filtration testing, indicating feed bottle change, permeate bottle change, process liquid flow, and sampling sequences. Note that the filtration of feed bottle “bottoms” began after 9.63 m^3/m^2 of feed had been filtered.

Table 4.1. System timeline.

Date	Time	Volume Filtered (m^3/m^2)	Event
14-Nov	9:46	0.00	Filtration started with BDEF-AP1-1
	10:05 - 11:12	0.07	Issue with MFC cable, reseat cable
	11:12	0.07	Resumed filtration
	13:24	0.41	Filtering from BDEF-AP1-2
	18:00	1.14	Filtering from BDEF-AP1-3
	18:25	1.21	IX-1 full, permeate switched to recycle for IX-1 replacement and sampling
	18:35	1.23	IX-2 in place, permeate switched for collection
	23:25	2.00	Filtering from BDEF-AP1-4
15-Nov	2:38	2.51	IX-2 full, permeate switched to recycle for IX-3 replacement
	2:44	2.52	IX-3 in place, permeate switched for collection
	4:56	2.87	Filtering from BDEF-AP1-5
	9:55	3.66	Filtering from BDEF-AP1-6
	10:47	3.80	IX-3 full, switched to IX-4
	15:10	4.49	Filtering from BDEF-AP1-7
	18:51	5.08	IX-4 full, permeate switched to recycle
	18:56	5.09	IX-5 in place, permeate switched for collection
	20:30	5.19	Filtering from BDEF-AP1-8
16-Nov	2:51	6.34	Filtering from BDEF-AP1-9
	2:59	6.36	IX-5 full, permeate switched to recycle
	3:04	6.38	IX-6 in place, permeate switched for collection
	4:28	6.60	TI-125-P2 sample taken from IX-6
	7:12	7.03	Filtering from BDEF-AP1-10
	11:03	7.64	IX-6 full, permeate switched to recycle
	11:05	7.65	IX-7 in place, permeate switched for collection
	12:53	7.93	Filtering from BDEF-AP1-11
	18:30	8.82	Filtering from BDEF-AP1-12
	19:10	8.92	IX-7 full, permeate switched to recycle
	19:12	8.93	IX-8 in place, permeate switched for collection
	23:38	9.63	Filtering from BDEF-AP1-1 “bottoms”
17-Nov	3:22	10.22	IX-8 full, permeate switched to recycle
	3:24	10.23	IX-9 in place, permeate switched for collection
	6:35	10.73	Filtering from BDEF-AP1-2 “bottoms”
	11:53	11.57	IX-9 full, permeate switched to recycle
	11:55	11.57	IX-10 in place, permeate switched for collection
	13:14	11.89	Feed bottle BDEF-AP1-2 bottom mixed and poured into reservoir
	20:02	12.86	IX-10 full, permeate switched to recycle
	20:03	12.86	IX-11 in place, permeate switched for collection
	21:37	13.05	End of filtration
	21:40	-	Backpulse at 80 psi
	22:08	-	Cleaned filter with 0.1 M NaOH (20-min recirculation, 2-h soak)
18-Nov	0:25	-	Backpulsed at 30 psi
	2:14	-	System shutdown

Testing was started on the morning of November 14 at 9:46 a.m. Shortly after filtration began, testing was paused from 10:05 a.m. to 11:12 a.m. after an issue with permeate control was observed. During troubleshooting, it was determined that the cause was a loose connection in the MFC cable inside the hot cell. The cable was reseated, and filtering continued at 11:12 a.m. Shortly following the first feed bottle change after 3.9 hours of operation (0.45 m^3/m^2 volume filtered), there was a minor spike in filter resistance, as seen in Figure 4.2. The resistance peaked at 7.60×10^9 m^{-1}, coinciding with increases in permeate density and recirculation pressure, before resuming to previous levels of ~5.0×10^9 m^{-1}. Filter resistance continued to gradually increase through 9.5 hours of operation (1.36 m^3/m^2 filtered), where it then stayed between ~1.0×10^{10} m^{-1} and 1.13×10^{10} m^{-1} through 32.5 hours of operation (4.98 m^3/m^2 filtered).

A minor drop in filter resistance is seen at 36 hours of operation (5.53 m^3/m^2 filtered), due to manually decreasing the BDEF slurry recirculation loop pressure to test the transmembrane pressure response. Similarly, a significant spike in resistance is seen at 7 m^3/m^2 volume filtered, due to manual testing of the transmembrane pressure response. Testing was done by incrementally adjusting the permeate flow rate from 1.00 to 5.0 mL/min using the MFC controller as shown in Figure 4.3. This was completed due the lack of differential pressure increase seen across the filter compared to previous BDEF filtering operations. The pressure differential response to the flow rate changes was considered satisfactory and deemed an accurate representation of the filter processing.

Three further spikes and subsequent drops in resistance are seen after 51.7 hours (8.01 m^3/m^2 volume filtered), 67.4 hours (10.50 m^3/m^2 volume filtered), and 78.4 hours (12.24 m^3/m^2 volume filtered) with resistance reaching a peak of 1.80×10^{10} m^{-1}. The three spikes follow trends seen in the spike at 0.45 m^3/m^2 volume filtered, with sudden increases in density and recirculation pressure. The recirculation pressure was manually adjusted each time.

Figure 4.2. AP-101 density during filtration process.

The density of the diluted AP-101 solution oscillated between approximately 1.26 and 1.28 g/mL as shown in Figure 4.2. The oscillation corresponds to a sudden spike in density with each changing of the BDEF feed bottle. Following the initial spikes in density, there are ensuing plateaus and drops in density for each of the feed bottles, indicating a non-homogenous solution and insufficient mixing during the dilution process. A large increase in density occurred at approximately 9.62 m^3/m^2 feed filtered with the feed bottle switch to BDEF-AP1-1 “bottoms,” eventually plateauing at approximately 1.35 g/mL. This further indicates the non-homogeneity of the diluted AP-101 solution, due to the consolidated bottoms of each feed bottle having a higher density than the previous volume that was filtered.

Transmembrane pressure and permeate flow rate through the testing campaign are shown in Figure 4.3. Average transmembrane pressure was 0.21 psid, with pressure spikes observed during adjustment of the recirculation loop pressure as previously mentioned.

Post filtration analysis of the product bottles prior to IX included the measurement of product density. Density measurement was performed in a 10-mL volumetric flask at ambient cell temperature of 24.0 °C. These values are reported in Table 4.2 and again show the variation in density observed from the MFC measurements during filtration.

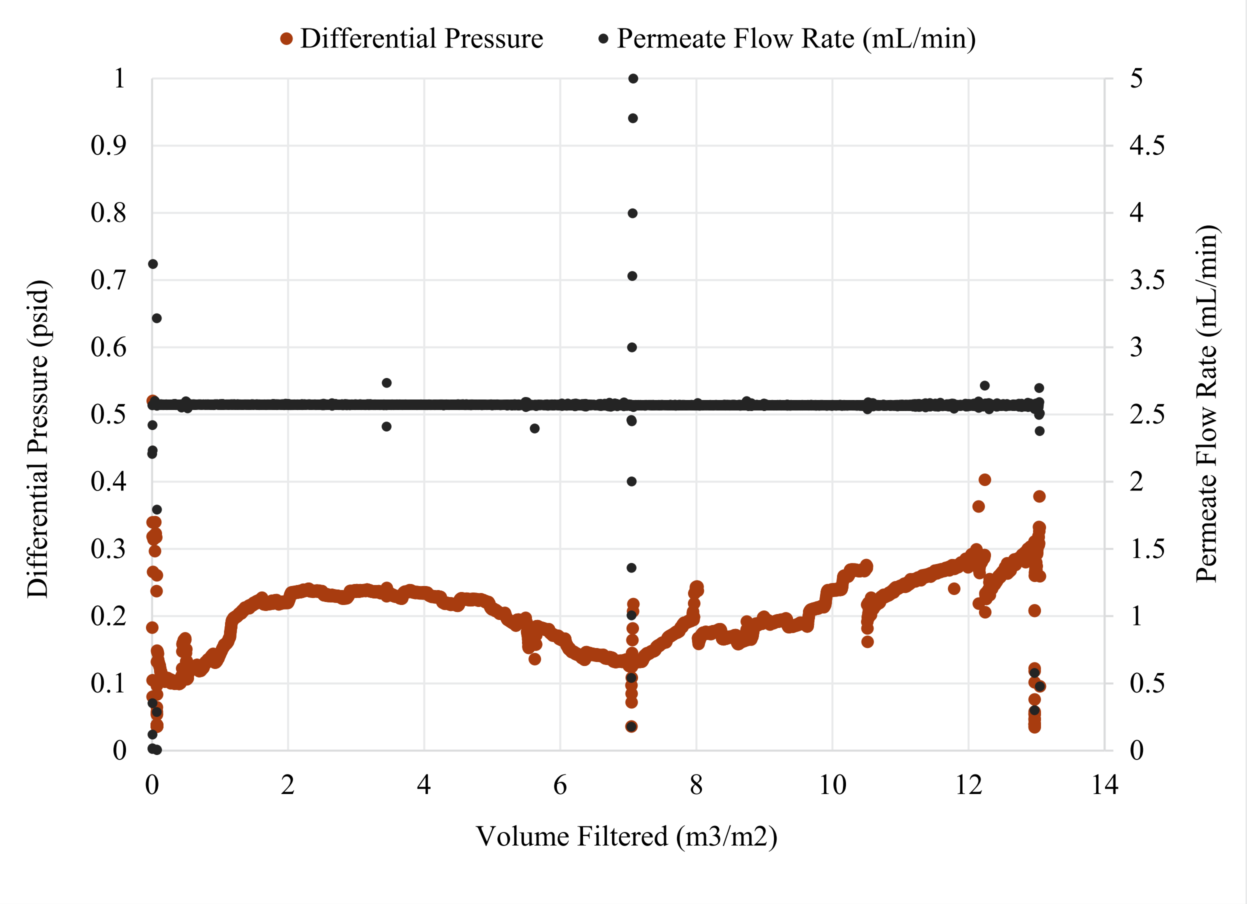

Figure 4.3. Filter differential pressure and MFC flow rate during waste filtering operations.

Table 4.2. Post filtration density measurements of product bottles.

Bottle ID	Density (g/mL)
IX-AP1-1	1.2584
IX-AP1-2	1.2440
IX-AP1-3	1.2337
IX-AP1-4	1.2398
IX-AP1-5	1.2385
IX-AP1-6	1.2697
IX-AP1-7	1.2458
IX-AP1-8	1.2488
IX-AP1-9	1.3042
IX-AP1-10	1.3155
IX-AP1-11	1.3172

4.4 Final CWF

At the conclusion of AP-101 filtration, a second cleaning was performed, and the CWF was measured again. Figure 4.4 compares this final CWF with the initial CWF. The filter differential pressure was lower during the final CWF, indicating that the second cleaning dissolved much of the solids that were deposited on the filter.

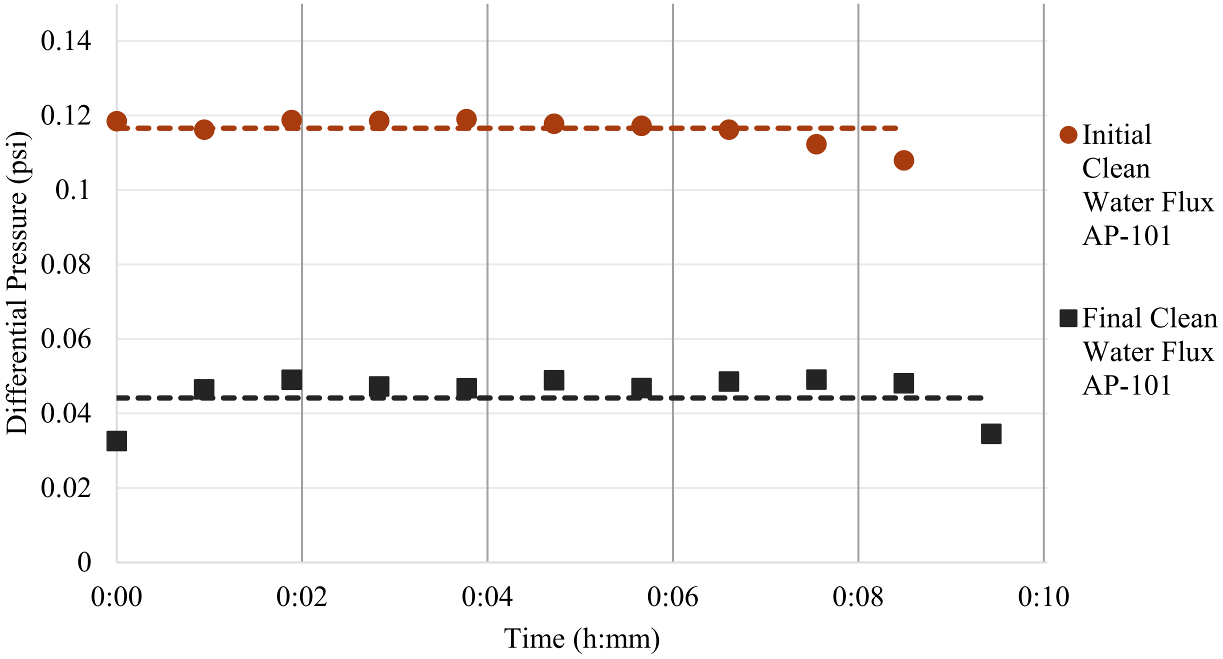

Figure 4.4. Initial and final clean water flux.

4.5 Analytical Results

4.5.1 River Water Analysis

Results of the ICP-OES analyses for the Columbia River water used for feed dilution are provided in Table 4.3 on a mass-per-unit volume basis (µg/mL). Some analyte results are shown in brackets; this indicates that the analytical result was less than the estimated quantitation limit but greater than or equal to the method detection limit and the associated analytical uncertainty could be higher than ±15%. All AOIs were measured to be present in the river water, excluding Zn. Other analytes measured are also included in the results. The top five components measured in the river water were Si, Na, B, Ca, and S. However, the elevated Si, Na, and B concentrations have been attributed to leaching from a glass vial used for the analytical subsample.

Table 4.3. ICP-OES analyte concentration in river water (ASR 1393).

	Concentration (µg/mL)
Si	66.0
Na	60.8
B	47.4
Ca	21.9
S	[9.15]
Mg	5.26
Al	3.37
As	[1.8]
K	[1.5]
W	[0.45]
Ru	[0.17]
Sr	0.130
Cu	[0.11]
Zr	[0.057]
V	[0.056]
Ba	0.0468
Li	[0.046]
Fe	[0.043]
Ti	[0.034]
Zn	--

Bracketed results were less than the estimated quantification limit but greater than or equal to the method detection limit and analytical uncertainty could be higher than ±15%.
"--" indicates that the concentration was less than the method detection limit.

4.5.2 As-Received AP-101 Supernate Tank Waste Analysis

ICP-OES and ICP-MS analyses were conducted on the as-received AP-101 supernate tank waste on a mass-per-unit-mass basis (µg/g) as presented in Table 4.4. Subsequently, the molarity of the as-received waste was calculated using a density of 1.3981 g/mL, which was determined upon receipt of the AP-101 tank waste.

The molarity was calculated using the following equation:

$$M = \frac{(m * \rho)}{MW}$$

Where M is the molarity, m is the mass, ρ is the density, and MW is the molecular weight of the component.

Table 4.4. ICP-OES and ICP-MS results of as-received AP-101 supernate tank waste.

Analysis Method	Analyte	As-Received AP-101 (µg/g)	As-Received AP-101 Molarity (mol/L)
ICP-OES	Na	146,149	8.89E00
	Al	11,412	5.91E-01
	K	4199	1.50E-01
	S	1842	4.11E-02
	Cr	603	1.62E-02
ICP-MS	Tc	10.2	1.43E-04

4.5.3 Total Alpha Energy Analysis

Total alpha analysis (alpha energy analysis, AEA) was conducted to determine the TRU content of the filtered permeate. The analysis results are given in Table 4.4 and show no gross breakthrough of TRU components that aren't already soluble. All samples remained below the 0.1 µCi/g threshold defining TRU waste per DOE M 435.1-1, *Radioactive Waste Management Manual*. The third permeate sample did show a higher alpha concentration, likely due to the consolidation of the product feed bottoms throughout filtration, as discussed in Section 4.3.

Table 4.5. AEA for permeate samples.

Analysis Method	Sample ID	(µCi/mL)	(µCi/g)
Total alpha analysis	TI-125-P1	4.02E-04	3.19E-04
	TI-125-P2	2.48E-04	1.97E-04
	TI-125-P3	1.43E-03	1.14E-03

4.5.4 Rheology Analysis of Filtered and Cesium Decontaminated AP-101 Supernate Tank Waste

The viscosity of the filtered and cesium exchanged AP-101 supernatant was measured with a Haake M5-RV20 (equipped with an M5 measuring head and RC20 controller) and an MV1 rotor and cup measuring system. Temperature control was achieved using a combination of the standard measuring system temperature jacket and a NESLAB Temperature-Controlled Circulator, Model Number RTE 111. This circulator allows heating and cooling of recirculation fluid to the rheometer over -25 to 150 °C with a stability of ± 0.01° C. Performance checks using a Cannon certified viscosity reference standard (Cannon Instrument Company) were carried out prior to and post measurements to verify that the system was functioning as expected. Viscosity was measured using a standard flow curve protocol comprising an up-ramp from 0 to 1000 s^{-1} for 5 minutes, a hold of 60 seconds at 1000 s^{-1}, and a finally down-ramp from 1000 to 0 s^{-1} over 5 minutes. Flow curves were measured at four temperatures: 10, 16, 25, and 35 °C. For each temperature, the Newtonian viscosity[1] of the liquid was determined by linear regression of the down-ramp data. The range of fit shear rates was generally limited to shear rates below 600 s^{-1} to exclude data impacted by onset of secondary flows (i.e., Taylor vortices). The results of linear regression analysis and the resulting best fit Newtonian viscosities are reported in Table 4.6. In all cases, the measured viscosity of the AP-101 supernatant is below the recommended measuring range of the measuring system (nominally 5.5 to 650 mPa s).

---

[1] While the AP-101 supernatant is expected to be Newtonian, linear regression analysis allowed for non-zero intercept to accommodate a non-zero torque offset introduced by the operator to accommodate negative torques resulting from operating the M5 viscometer outside its standard operating range (in this case, for viscosities below 5.5 mPa s).

Table 4.6. Viscosity results of filtered and Cs decontaminated sample.

Temperature, °C	Fit Range Down-Ramp, s^{-1}	Yield Stress Pa	Viscosity mPa s	Viscosity Uncertainty[a] 3-Sigma Relative % Standard Error
10	0-600	0	3.742	4.057
16	0-600	0	3.116	3.902
25	0-600	0.0466	2.667	6.522
35	0-500	0.0250	2.401	12.21

(a) The uncertainty reported by the Haake software for the curve fit is the 3-sigma relative percent standard error.

4.6 Microscopy Solids Analysis

Material collected from the concentrated backpulse solution was submitted for examination by SEM and higher-resolution scanning transmission electron microscopy (STEM). A full report of the particle analysis can be found in Appendix E. The automated particle analysis routines used in this work enabled significant improvements in the representativeness of collected SEM data as the work can be performed unattended and in a non-biased fashion.

The solids observed in the filtered solutions consisted of large blocky particles (see Figure 4.5). Compositional analysis with X-ray energy dispersive spectroscopy indicated the phases consisted mainly of sodium and nitrogen bearing phases. Aluminum and silicon bearing phases were also observed, and these were investigated more closely with STEM. Very few heavy elements were observed. The major phase was identified as $NaNO_3$ (from the washing solution used for sample preparation) with electron diffraction. Aluminum and silicon phases were identified as cancrinite.

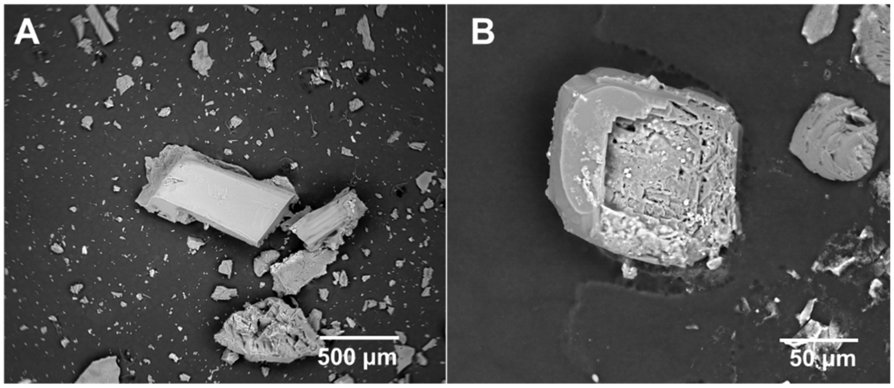

Figure 4.5. SEM images of example morphologies observed from the filtered AP-101 supernatant: (A) distribution of particles taken at low magnification, (B) high surface area agglomerate.

To improve the effectiveness of SEM studies, more detailed STEM analyses can provide missing information on specific questions, such as the concentration of light elements in a specific phase, electron diffraction analysis, and more targeted compositional analysis. The disadvantage of the STEM analysis is the limited area that it can examine, so it is a tool for confirming results from other methods (see Figure 4.6). Using automated routines, it was possible to look at the effect of exposing the filtered solids to deionized water. In Figure 4.7, the ternary plots show the change in average composition of the particles and the loss of sodium bearing phases.

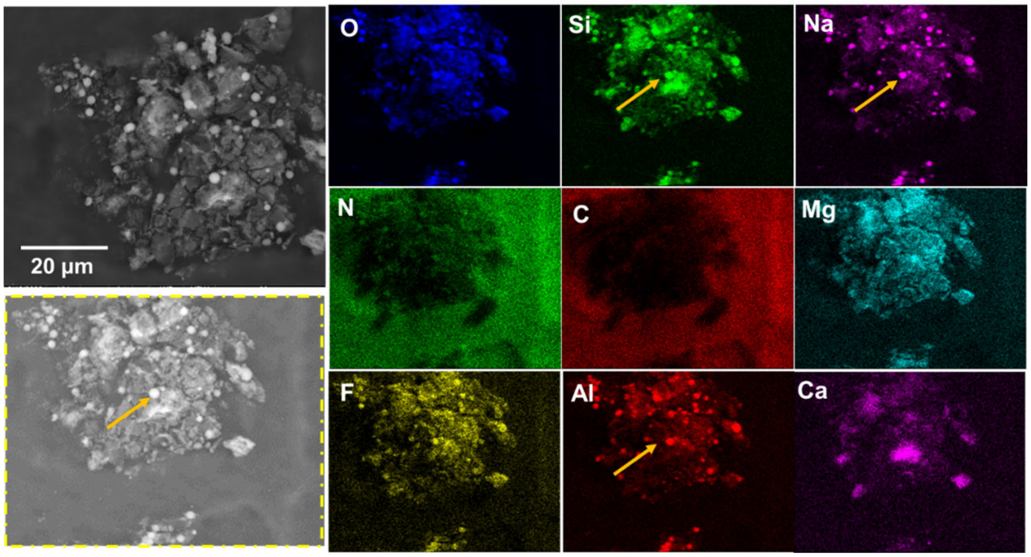

Figure 4.6. Backscatter electron (BSE) images and elemental maps of a particle agglomerate from AP-101 supernatant-solids. The elemental maps show the presence of a round aluminosilicate phase (indicated by arrow).

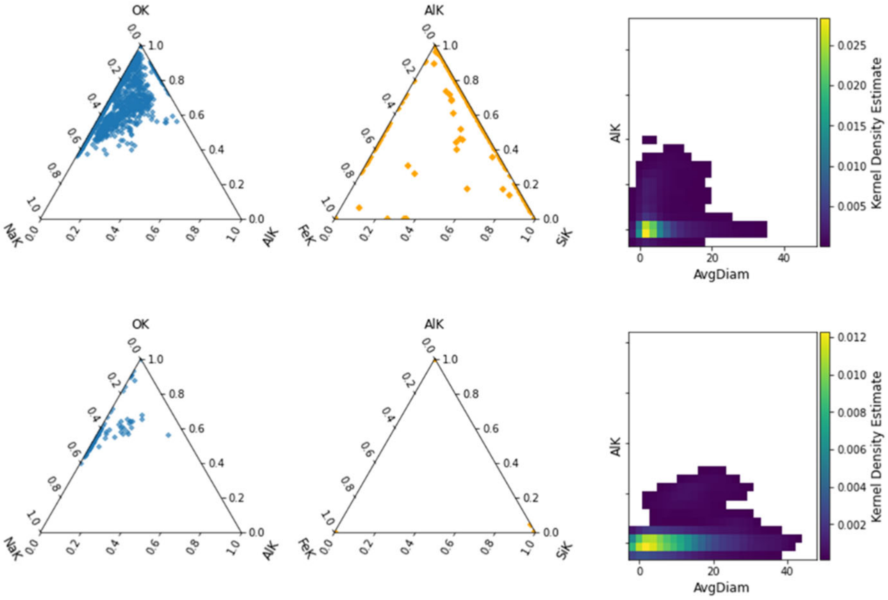

Figure 4.7. Effect of dissolution on the particle composition of AP-101 supernatant through ternary phase diagrams and compositional-particle size distributions, showing the loss of sodium bearing phases.

5.0 Conclusions

Based on the results of the filtration experiments on supernatant waste from tank 241-AP-101 at a lower operating temperature (16 °C), the following observations and conclusions were made:

- The Media Grade 5 BDEF filter was run at the TSCR targeted flux of 0.065 gpm/ft^2 and the filter exhibited little to no measurable increase in resistance over almost 84 hours of testing (and ~13 m^3 of permeate produced per m^2 of filter area).
- There were no observable solids in the AP-101 sample received. The BDEF filter was backpulsed after approximately 84 hours of filtration with a very small amount of observable solids in the backflush concentrate.
- Results indicate that the TSCR filter should perform well when processing AP-101 supernatant.
- Solids concentrated from the backpulse solutions displayed sodium nitrate-type phases, aluminum and silicon phases reported as cancrinite or nitrate-cancrinite, a mixed chromium-aluminum oxide, iron oxides, and Ca-bearing phases (calcite). The SEM analyses showed that the average particle size was 0.5 microns.

6.0 References

Allred JR, JGH Geeting, AM Westesen, EC Buck, and RA Peterson. 2021. *Fiscal Year 2021 Filtration of Hanford Tank 241-AP-107 Supernatant Samples Obtained at Prototypic Tank Level and Filtered at 16 °C*. PNNL-31557, Rev. 0 (RPT-DFTP-028, Rev. 0). Pacific Northwest National Laboratory, Richland, Washington.

Allred JR, JGH Geeting, AM Westesen, EC Buck, and RA Peterson. 2020. *Fiscal Year 2020 Filtration of Hanford Tank Waste 241-AP-105*. PNNL-30485, Rev. 0 (RPT-DFTP-021, Rev. 0). Pacific Northwest National Laboratory, Richland, Washington.

ASME. 2000. *Quality Assurance Requirements for Nuclear Facility Applications*. NQA-1-2000. The American Society of Mechanical Engineers, New York, New York.

ASME. 2008. *Quality Assurance Requirements for Nuclear Facility Applications*. NQA-1-2008. The American Society of Mechanical Engineers, New York, New York.

ASME. 2009. *Addenda to ASME NQA-1-2008*. NQA-1a-2009. The American Society of Mechanical Engineers, New York, New York.

Geeting JGH, JR Allred, AM Rovira, and RA Peterson. 2019. *Fiscal Year 2019 Filtration of Hanford Tank AP-107 Supernatant*. PNNL-28780, Rev. 0 (RPT-DFTP-015, Rev. 0). Pacific Northwest National Laboratory, Richland, Washington.

Geeting JGH, AM Rovira, JR Allred, RW Shimskey, CA Burns, and RA Peterson. 2018a. *Filtration of Hanford Tank AP-107 Supernatant*. PNNL-27638 (RPT-DFTP-009, Rev. 0). Pacific Northwest National Laboratory, Richland, Washington.

Geeting JGH, JR Allred, AM Rovira, RW Shimskey, CA Burns, and RA Peterson. 2018b. *Crossflow Filtration of Hanford Tank AP-105 Supernatant*. PNNL-27085 (RPT-DFTP-005, Rev. 0). Pacific Northwest National Laboratory, Richland, Washington.

Gerber MS. 1992. *Legend and Legacy: Fifty Years of Defense Production at the Hanford Site*. WHC-MR-0293, Rev. 2. Westinghouse Hanford Company, Richland, Washington. doi:10.2172/10144167

Appendix A – BDEF Piping and Instrumentation Diagram

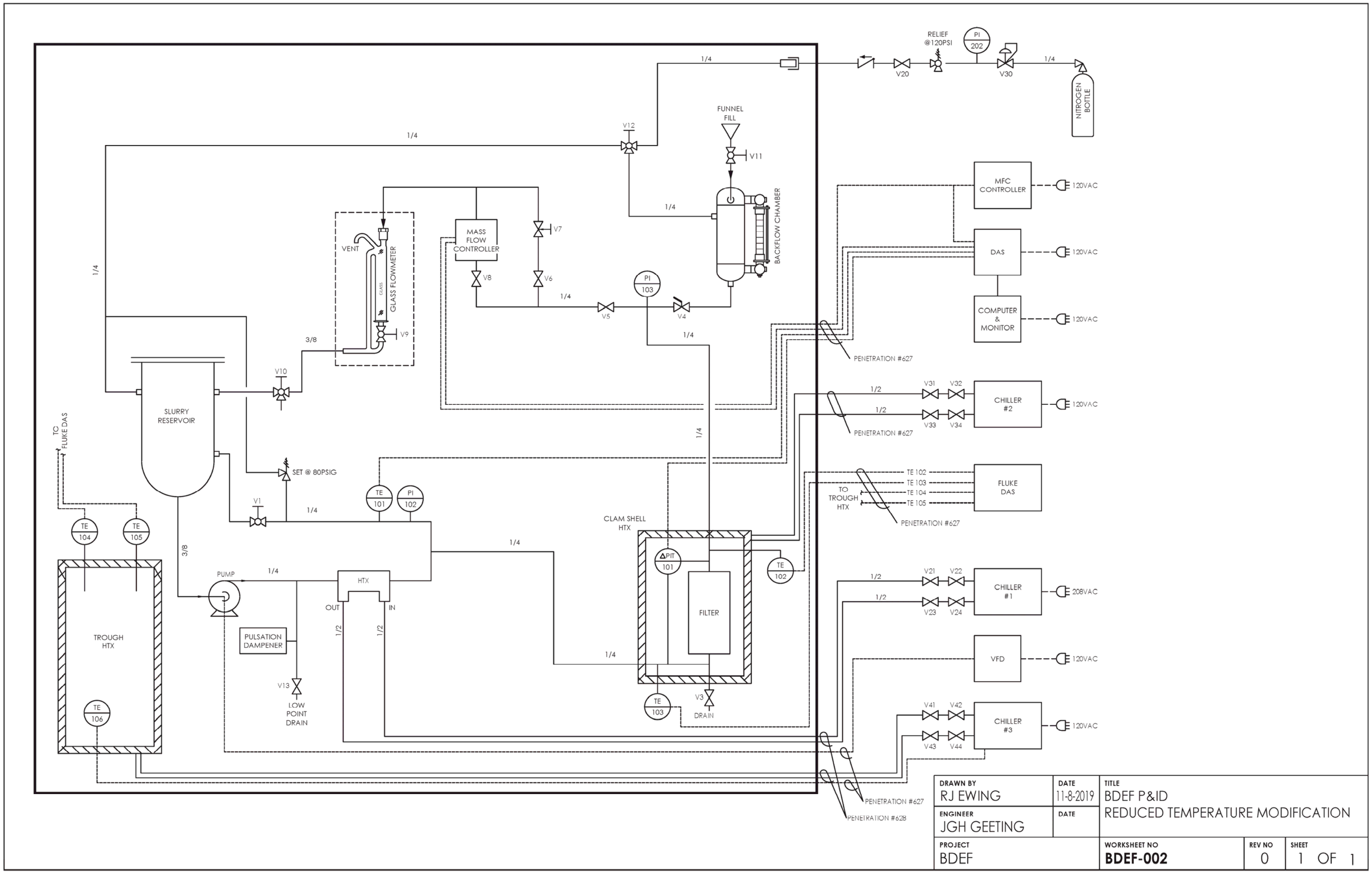

Figure A.1. BDEF piping and instrumentation diagram.

Appendix B – Total Alpha Analysis for Filtration Permeate Samples

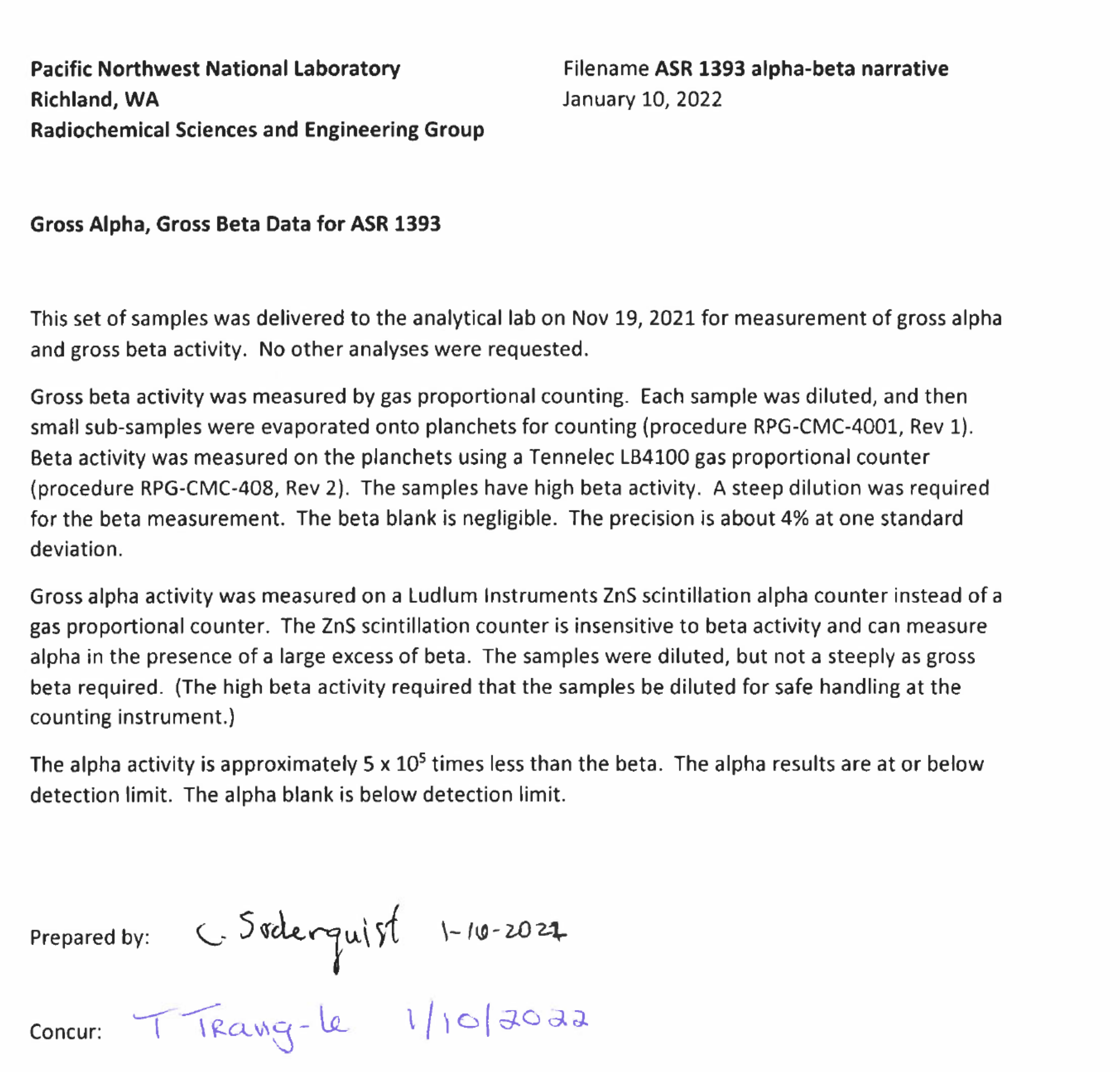

Pacific Northwest National Laboratory
Richland, WA
Radiochemical Sciences and Engineering Group

Filename **ASR 1393 alpha-beta narrative**
January 10, 2022

Gross Alpha, Gross Beta Data for ASR 1393

This set of samples was delivered to the analytical lab on Nov 19, 2021 for measurement of gross alpha and gross beta activity. No other analyses were requested.

Gross beta activity was measured by gas proportional counting. Each sample was diluted, and then small sub-samples were evaporated onto planchets for counting (procedure RPG-CMC-4001, Rev 1). Beta activity was measured on the planchets using a Tennelec LB4100 gas proportional counter (procedure RPG-CMC-408, Rev 2). The samples have high beta activity. A steep dilution was required for the beta measurement. The beta blank is negligible. The precision is about 4% at one standard deviation.

Gross alpha activity was measured on a Ludlum Instruments ZnS scintillation alpha counter instead of a gas proportional counter. The ZnS scintillation counter is insensitive to beta activity and can measure alpha in the presence of a large excess of beta. The samples were diluted, but not a steeply as gross beta required. (The high beta activity required that the samples be diluted for safe handling at the counting instrument.)

The alpha activity is approximately 5 x 10^5 times less than the beta. The alpha results are at or below detection limit. The alpha blank is below detection limit.

Prepared by: C. Soderquist 1-10-2022

Concur: T Trang-le 1/10/2022

Pacific Northwest National Laboratory **Richland, WA** **Radiochemical Sciences and Engineering Group**	filename 21-0168 Geeting 12/21/2021

Client: J. Geeting   Project: 79156
ASR 1393   WP#: NK4628

Prepared by: T Trang-Le 12/21/21
Technical Reviewer: C Soderquist 12-21-2021

Procedures:	RPG-CMC-4001, Rev 1, Source Preparation for Gross Alpha and Gross Beta Analysis RPG-CMC-408, Rev 2, Total Alpha and Total Beta Analysis
M&TE:	LB4100 beta proportional counters, Ludlum
Count dates:	12/07 to 12/21/21

	Lab	**Measured Activity, µCi/mL ± 1s**			
Sample	ID	**Gross alpha**		**Gross beta**	
TI-125-P1	22-0168	5.24E-4	± 26%	1.33E+2	± 4%
	22-0168 DUP	2.79E-4	± 41%	1.27E+2	± 4%
	RPD	61%		5%	
TI-125-P2	22-0169	2.48E-4	± 43%	1.25E+2	± 4%
TI-125-P3	22-0170	1.43E-3	± 14%	1.82E+2	± 4%
	Reagent Spike	98%		105%	
	Matrix Spike	86%		80%	
	Blank	7.4E-8	± 541%	4.3E-6	± 75%

Appendix C – ICP-OES Analysis for Raw Columbia River Water

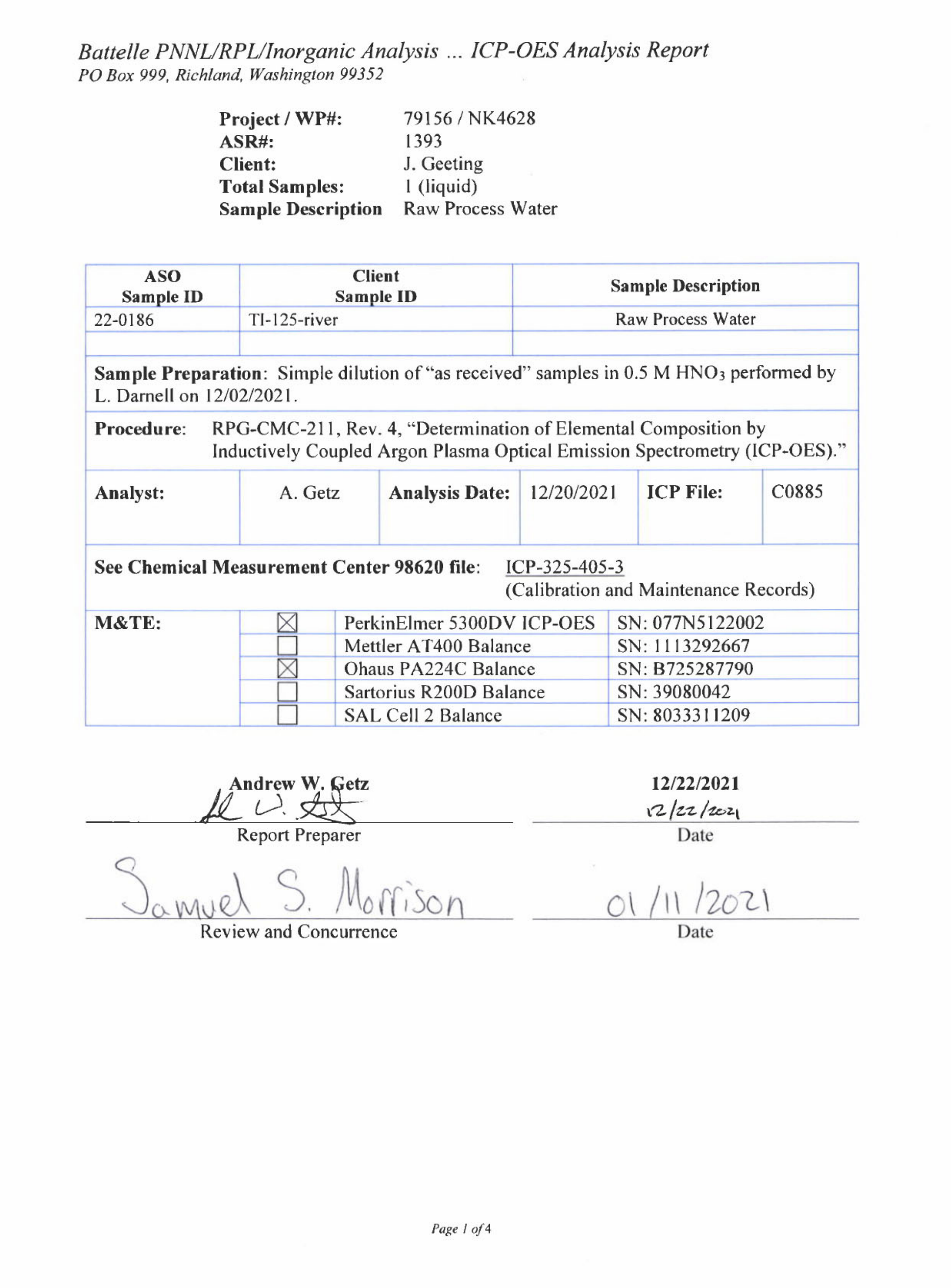

Battelle PNNL/RPL/Inorganic Analysis ... ICP-OES Analysis Report
PO Box 999, Richland, Washington 99352

Project / WP#:	79156 / NK4628
ASR#:	1393
Client:	J. Geeting
Total Samples:	1 (liquid)
Sample Description	Raw Process Water

ASO Sample ID	Client Sample ID	Sample Description
22-0186	TI-125-river	Raw Process Water

Sample Preparation: Simple dilution of "as received" samples in 0.5 M HNO_3 performed by L. Darnell on 12/02/2021.

Procedure: RPG-CMC-211, Rev. 4, "Determination of Elemental Composition by Inductively Coupled Argon Plasma Optical Emission Spectrometry (ICP-OES)."

Analyst:	A. Getz	**Analysis Date:**	12/20/2021	**ICP File:**	C0885

See Chemical Measurement Center 98620 file: ICP-325-405-3 (Calibration and Maintenance Records)

M&TE:	☒	PerkinElmer 5300DV ICP-OES	SN: 077N5122002
	☐	Mettler AT400 Balance	SN: 1113292667
	☒	Ohaus PA224C Balance	SN: B725287790
	☐	Sartorius R200D Balance	SN: 39080042
	☐	SAL Cell 2 Balance	SN: 8033311209

Andrew W. Getz **12/22/2021**
12/22/2021
Report Preparer Date

Samuel S. Morrison 01/11/2021
Review and Concurrence Date

Page 1 of 4

Battelle PNNL/RPL/Inorganic Analysis ... ICP-OES Analysis Report

One liquid sample was submitted under Analytical Service Request (ASR) 1393 and analyzed by ICP-OES. The samples were analyzed after dilution of the "as received" liquid in 0.5 M HNO_3. Neither the sample nor any of the dilutions were filtered.

All sample results are reported on a mass per unit volume basis (µg/mL) for each detected analyte. The data have been adjusted for instrument dilutions.

Analytes of interest (AOI) were specified in the ASR and are listed in the upper section of the attached ICP-OES Data Report. The quality control (QC) results for the AOI have been evaluated and are presented below. Analytes other than the AOI are reported in the bottom section of the report but have not been fully evaluated for QC performance.

Calibration of the ICP-OES was done following the manufacturer's recommended calibration procedure using multi-analyte custom standard solutions traceable to the National Institute of Standards and Technology (NIST). Midrange calibration verification standards (MCVA and MCVB) were used to verify acceptance of the two-point calibration curves obtained for each analyte and for continuing calibration verification.

The controlling documents were procedures RPG-CMC-211, Rev. 4, *Determination of Elemental Composition by Inductively Coupled Argon Plasma Optical Emission Spectrometry (ICP-OES)*, and ASO-QAP-001, Rev. 11, *Analytical Support Operations (ASO) Quality Assurance Plan*. Instrument calibrations, QC checks and blanks (e.g., ICV/ICB, CCV/CCB, LLS, ICS), matrix spike, post-digestion spikes, duplicate, reagent spike, blank spike, and serial dilution were conducted during the analysis run.

Preparation Blank (PB):

No preparation blank was required. The ICP-OES laboratory diluent (5% HNO_3) was analyzed as a blank. All AOI were within the acceptance criteria of <EQL (estimated quantitation level), <50% regulatory decision level, or less than ≤10% of the concentration in the samples.

Blank Spike (BS)/Laboratory Control Sample (LCS):

A 50:50 mixture of the MCVA and MCVA solutions was analyzed as the blank spike. Recovery values are listed for all analytes included in the BS that were measured at or above the EQL. All AOI were present in the MCVA solution. Recovery values for the AOI meeting this requirement were within the acceptance criterion of 80% to 120%.

Replicate Relative Percent Difference (RPD)/Relative Standard Deviation (RSD):

A duplicate of sample 22-0186 was prepared and analyzed. RPDs are listed for all analytes that were measured at or above the EQL. RPDs for the AOI meeting this requirement ranged from 0.2% to 6.9% and were within the acceptance criterion of ≤20% for liquid samples.

Matrix-Spike (MS) Sample:

No matrix spike was required.

Initial/Continuing Calibration Verification (ICV/CCV):

MCVA and MCVB solutions were analyzed immediately after calibration, after each group of not more than ten samples, and at the end of the analytical run. The concentrations of all AOI were within the acceptance criteria of 90% to 110% recovery.

Initial/Continuing Calibration Blank (ICB/CCB):

The ICB/CCB solution (5% v/v HNO_3) was analyzed immediately after the ICV solutions and after the CCV solutions (after each group of not more than ten samples and at the end of the analytical run). The concentration of all AOI were within the acceptance criteria of <EQL.

Low-Level Standard (LLS):

The LLS solution was analyzed immediately after the first CCB solution. The concentrations of all AOI were within the acceptance criteria of 70% to 130% recovery.

Interference Check Standard (ICS/SST):

The ICS solution was analyzed immediately after the first LLS solution and immediately prior to analyzing the final CCV solutions. The concentrations of all AOI were within the acceptance criteria of 80% to 120% recovery.

Analytical Spike (AS-A) - Sample (A Component):

An analytical spike (A Component) was conducted on sample 22-0186. Recovery values are listed for all analytes in the spike that were measured at or above the EQL, and that had a spike concentration ≥25% of that in the sample. Recovery values for the AOI meeting this requirement were 101% to 105% and within the acceptance criterion of 80% to 120%.

Analytical Spike (AS-B) - Sample (B Component):

An analytical spike (B Component) was conducted on sample 22-0186. Recovery values are listed for all analytes in the spike that were measured at or above the EQL, and that had a spike concentration ≥25% of that in the sample. Recovery values for the AOI meeting this requirement was 97% and within the acceptance criterion of 80% to 120%.

Serial Dilution (SD):

Five-fold serial dilution was conducted on sample 22-0186. Percent differences (%Ds) are listed for all analytes that had a concentration at or above the EQL in the diluted sample. The %Ds for the AOI meeting this requirement ranged from 0.1% to 5.9% and were within the acceptance criterion of ≤10%.

Other QC:

All other instrument-related QC tests for the AOI passed within their respective acceptance criteria.

Battelle PNNL/RPL/Inorganic Analysis ... ICP-OES Analysis Report

Comments:

1) The "Final Results" have been corrected for all laboratory dilutions performed on the samples during processing and analysis, unless specifically noted.
2) Instrument detection limits (IDL) and estimated quantitation limits (EQL) shown are for acidified water and/or fusion flux matrices as applicable. Method detection limits (MDL) for individual samples can be estimated by multiplying the IDL by the "Process Factor" for that individual sample. The estimated quantitation limit (EQL) for each concentration value can be obtained by multiplying the EQL by the "Process Factor".
3) Routine precision and bias is typically ±15% or better for samples in dilute, acidified water (e.g. 5% v/v HNO_3 or less) at analyte concentrations > EQL up to the upper calibration level. This also presumes that the total dissolved solids concentration in the sample is less than 5000 µg/mL (0.5 per cent by weight). Note that bracketed values listed in the data report are within the MDL and the EQL, and have potential uncertainties greater than 15%. Concentration values < MDL are listed as "- -". Note, that calibration and QC standard samples are validated to a precision of ±10%.
4) Analytes included in the spike A component (for the AS/PS) are; Ag, Al, As, B, Ba, Be, Bi, Ca, Cd, Co, Cr, Cu, Fe, K, Li, Mg, Mn, Mo, Na, Ni, P, Pb, Sb, Se, Si, Sn, Sr, Ta, Ti, Tl, V, W, Y, Zn, and Zr. Analytes included in the spike B component are; Ce, Dy, Eu, La, Nd, Pd, Rh, Ru, S, Te, Th, and U.

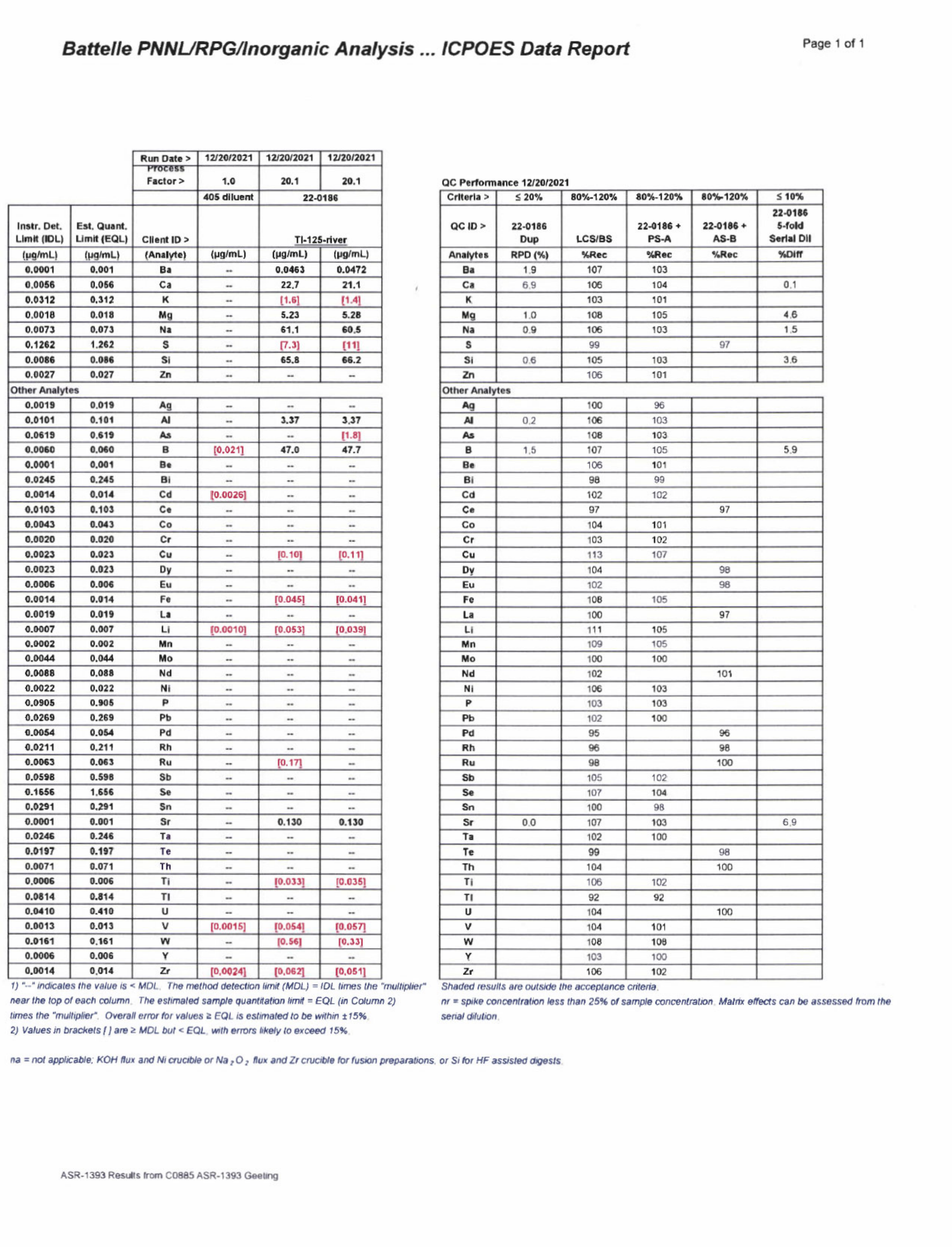

Battelle PNNL/RPG/Inorganic Analysis ... ICPOES Data Report

Page 1 of 1

		Run Date >	12/20/2021	12/20/2021	12/20/2021
		Process Factor >	1.0	20.1	20.1
			405 diluent	22-0186	
Instr. Det. Limit (IDL)	Est. Quant. Limit (EQL)	Client ID >		TI-125-river	
(µg/mL)	(µg/mL)	(Analyte)	(µg/mL)	(µg/mL)	(µg/mL)
0.0001	0.001	Ba	--	0.0463	0.0472
0.0056	0.056	Ca	--	22.7	21.1
0.0312	0.312	K	--	[1.6]	[1.4]
0.0018	0.018	Mg	--	5.23	5.28
0.0073	0.073	Na	--	61.1	60.5
0.1262	1.262	S	--	[7.3]	[11]
0.0086	0.086	Si	--	65.8	66.2
0.0027	0.027	Zn	--	--	--
Other Analytes					
0.0019	0.019	Ag	--	--	--
0.0101	0.101	Al	--	3.37	3.37
0.0619	0.619	As	--	--	[1.8]
0.0060	0.060	B	[0.021]	47.0	47.7
0.0001	0.001	Be	--	--	--
0.0245	0.245	Bi	--	--	--
0.0014	0.014	Cd	[0.0026]	--	--
0.0103	0.103	Ce	--	--	--
0.0043	0.043	Co	--	--	--
0.0020	0.020	Cr	--	--	--
0.0023	0.023	Cu	--	[0.10]	[0.11]
0.0023	0.023	Dy	--	--	--
0.0006	0.006	Eu	--	--	--
0.0014	0.014	Fe	--	[0.045]	[0.041]
0.0019	0.019	La	--	--	--
0.0007	0.007	Li	[0.0010]	[0.053]	[0.039]
0.0002	0.002	Mn	--	--	--
0.0044	0.044	Mo	--	--	--
0.0088	0.088	Nd	--	--	--
0.0022	0.022	Ni	--	--	--
0.0905	0.905	P	--	--	--
0.0269	0.269	Pb	--	--	--
0.0054	0.054	Pd	--	--	--
0.0211	0.211	Rh	--	--	--
0.0063	0.063	Ru	--	[0.17]	--
0.0598	0.598	Sb	--	--	--
0.1656	1.656	Se	--	--	--
0.0291	0.291	Sn	--	--	--
0.0001	0.001	Sr	--	0.130	0.130
0.0246	0.246	Ta	--	--	--
0.0197	0.197	Te	--	--	--
0.0071	0.071	Th	--	--	--
0.0006	0.006	Ti	--	[0.033]	[0.035]
0.0814	0.814	Tl	--	--	--
0.0410	0.410	U	--	--	--
0.0013	0.013	V	[0.0015]	[0.054]	[0.057]
0.0161	0.161	W	--	[0.56]	[0.33]
0.0006	0.006	Y	--	--	--
0.0014	0.014	Zr	[0.0024]	[0.062]	[0.051]

1) "--" indicates the value is < MDL. The method detection limit (MDL) = IDL times the "multiplier" near the top of each column. The estimated sample quantitation limit = EQL (in Column 2) times the "multiplier". Overall error for values ≥ EQL is estimated to be within ±15%.

2) Values in brackets [ ] are ≥ MDL but < EQL, with errors likely to exceed 15%.

QC Performance 12/20/2021

Criteria >	≤ 20%	80%-120%	80%-120%	80%-120%	≤ 10%
QC ID >	22-0186 Dup	LCS/BS	22-0186 + PS-A	22-0186 + AS-B	22-0186 5-fold Serial Dil
Analytes	RPD (%)	%Rec	%Rec	%Rec	%Diff
Ba	1.9	107	103		
Ca	6.9	106	104		0.1
K		103	101		
Mg	1.0	108	105		4.6
Na	0.9	106	103		1.5
S		99		97	
Si	0.6	105	103		3.6
Zn		106	101		
Other Analytes					
Ag		100	96		
Al	0.2	106	103		
As		108	103		
B	1.5	107	105		5.9
Be		106	101		
Bi		98	99		
Cd		102	102		
Ce		97		97	
Co		104	101		
Cr		103	102		
Cu		113	107		
Dy		104		98	
Eu		102		98	
Fe		108	105		
La		100		97	
Li		111	105		
Mn		109	105		
Mo		100	100		
Nd		102		101	
Ni		106	103		
P		103	103		
Pb		102	100		
Pd		95		96	
Rh		96		98	
Ru		98		100	
Sb		105	102		
Se		107	104		
Sn		100	98		
Sr	0.0	107	103		6.9
Ta		102	100		
Te		99		98	
Th		104		100	
Ti		106	102		
Tl		92	92		
U		104		100	
V		104	101		
W		108	108		
Y		103	100		
Zr		106	102		

Shaded results are outside the acceptance criteria.

nr = spike concentration less than 25% of sample concentration. Matrix effects can be assessed from the serial dilution.

na = not applicable; KOH flux and Ni crucible or Na_2O_2 flux and Zr crucible for fusion preparations, or Si for HF assisted digests.

ASR-1393 Results from C0885 ASR-1393 Geeting

Appendix D – ICP-OES Analysis for As-Received 241-AP-101 Supernatant

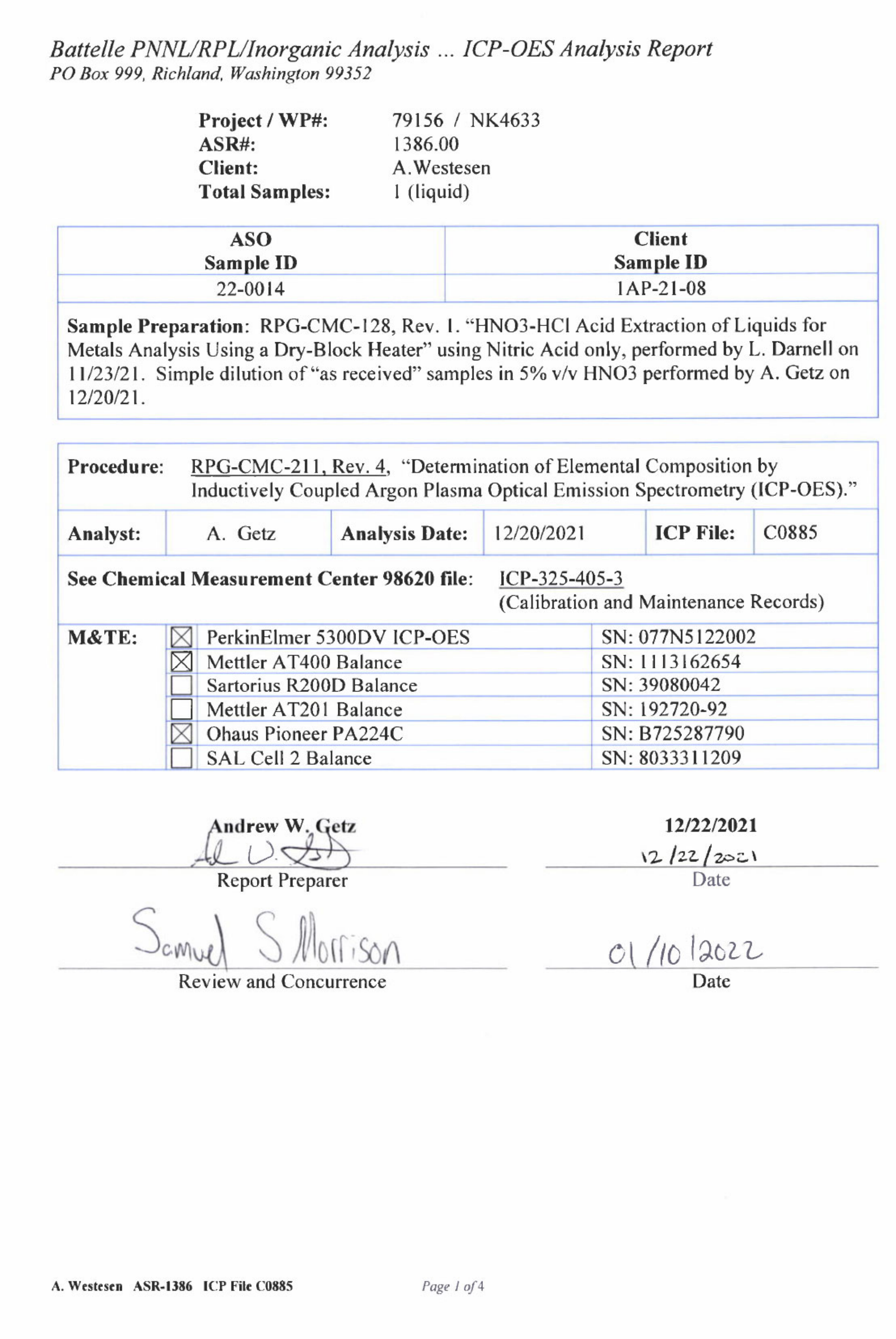

Battelle PNNL/RPL/Inorganic Analysis ... ICP-OES Analysis Report
PO Box 999, Richland, Washington 99352

Project / WP#: 79156 / NK4633
ASR#: 1386.00
Client: A.Westesen
Total Samples: 1 (liquid)

ASO Sample ID	Client Sample ID
22-0014	1AP-21-08

Sample Preparation: RPG-CMC-128, Rev. 1. "HNO3-HCl Acid Extraction of Liquids for Metals Analysis Using a Dry-Block Heater" using Nitric Acid only, performed by L. Darnell on 11/23/21. Simple dilution of "as received" samples in 5% v/v HNO3 performed by A. Getz on 12/20/21.

Procedure: RPG-CMC-211, Rev. 4, "Determination of Elemental Composition by Inductively Coupled Argon Plasma Optical Emission Spectrometry (ICP-OES)."

Analyst:	A. Getz	**Analysis Date:**	12/20/2021	**ICP File:**	C0885

See Chemical Measurement Center 98620 file: ICP-325-405-3
(Calibration and Maintenance Records)

M&TE:	☒	PerkinElmer 5300DV ICP-OES	SN: 077N5122002
	☒	Mettler AT400 Balance	SN: 1113162654
	☐	Sartorius R200D Balance	SN: 39080042
	☐	Mettler AT201 Balance	SN: 192720-92
	☒	Ohaus Pioneer PA224C	SN: B725287790
	☐	SAL Cell 2 Balance	SN: 8033311209

Andrew W. Getz — **12/22/2021**
12/22/2021
Report Preparer — Date

Samuel S Morrison — 01/10/2022
Review and Concurrence — Date

Battelle PNNL/RPL/Inorganic Analysis ... ICP-OES Analysis Report

One aqueous sample was submitted under Analytical Service Request (ASR) 1386 was analyzed by ICP-OES. The sample was prepared following RPL procedure RPG-CMC-128, Rev. 1, "HNO3-HCl Acid Extraction of Liquids for Metals Analysis Using a Dry-Block Heater". This process was conducted without the use of HCl. All samples were diluted in 5% HNO3 prior to analysis. None of the samples were filtered.

All sample results are reported on a mass per mass of sample prior to dissolution basis (µg/g) for each detected analyte. The data have been adjusted for instrument dilutions.

Analytes of interest (AOI) were specified in the ASR and are listed in the upper section of the attached ICP-OES Data Report. The quality control (QC) results for the AOI have been evaluated and are presented below. Analytes other than the AOI are reported in the bottom section of the report but have not been fully evaluated for QC performance.

Calibration of the ICP-OES was done following the manufacturer's recommended calibration procedure using multi-analyte custom standard solutions traceable to the National Institute of Standards and Technology (NIST). Midrange calibration verification standards (MCVA and MCVB) were used to verify acceptance of the two-point calibration curves obtained for each analyte and for continuing calibration verification.
The controlling documents were procedures RPG-CMC-211, Rev 4, *Determination of Elemental Composition by Inductively Coupled Argon Plasma Optical Emission Spectrometry (ICP-OES)*, and ASO-QAP-001, Rev. 11, *Analytical Support Operations (ASO) Quality Assurance Plan*. Instrument calibrations, QC checks and blanks (e.g., ICV/ICB, CCV/CCB, LLS, ICS), post-digestion spikes, duplicate, blank spike, and serial dilution were conducted during the analysis run.

Preparation Blank (PB):

A process blank was included with the sample set. All AOI were within the acceptance criteria of <EQL (estimated quantitation level), <50% regulatory decision level, or less than ≤10% of the concentration in the samples.

Reagent Spike (BS):

A reagent spike sample was prepared with samples and processed through the dissolution process. Recovery values are listed for all analytes included in the BS that were measured at or above the EQL. Recovery values for the AOI meeting this requirement were 98% - 99.9% and are all within the acceptance criterion of 80% to 120%.

Duplicate(Dup) Relative Percent Difference (RPD):

Duplicates of sample 22-0034 was prepared along with the samples and analyzed. The RPD ranged from 0.7% - 2.0% and were within the acceptance criterion of ≤20% for solid samples.

Matrix-Spike (MS) Sample:

A matrix spike was prepared using sample 22-0014. Recovery values are listed for all analytes included in the MS that were measured at or above the EQL. Recovery values for the AOI meeting this requirement were 100% - 102% and are all within the acceptance criterion of 75% to 125%.

Initial/Continuing Calibration Verification (ICV/CCV):

MCVA and MCVB solutions were analyzed immediately after calibration, after each group of not more than ten samples, and at the end of the analytical run. The concentrations of all AOI were within the acceptance criteria of 90% to 110%.

Initial/Continuing Calibration Blank (ICB/CCB):

The ICB/CCB solution (5% v/v HNO_3) was analyzed immediately after the ICV solutions and after the CCV solutions (after each group of not more than ten samples and at the end of the analytical run). The concentration of all AOI were within the acceptance criteria of <EQL.

Low-Level Standard (LLS):

The LLS solution was analyzed immediately after the first CCB solution. The concentrations of all AOI were within the acceptance criteria of 70% to 130% recovery.

Interference Check Standard (ICS/SST):

The ICS solution was analyzed immediately after the first LLS solution and immediately prior to analyzing the final CCV solutions. The concentrations of all AOI were within the acceptance criteria of 80% to 120% recovery.

Serial Dilution (SD):

Five-fold serial dilution was conducted on sample 22-0014. The percent difference (%D) for the AOIs ranged from 2.3% - 3.3% meeting the acceptance criteria of $\leq$ 10%.

Post-Digestion Spike (PS-A) - Sample (A Component):

In addition to the BS sample, a post-digestion spike (A Component) was conducted on sample 22-0014. The recovery for the AOIs ranged from 93% - 106% meeting the acceptance criterion of 99.8% to 100.2%.

Post-Digestion Spike (PS-B) - Sample (B Component):

In addition to the BS sample, a post-digestion spike (B Component) was conducted on sample 22-0014. There were no AOIs in the B Component, all non-AOI recoveries met the acceptance criterion of 80% to 120%.

Other QC:

All other instrument-related QC tests for the AOI passed within their respective acceptance criteria.

Comments:

Battelle PNNL/RPL/Inorganic Analysis ... ICP-OES Analysis Report

1) The "Final Results" have been corrected for all laboratory dilutions performed on the samples during processing and analysis, unless specifically noted.
2) Instrument detection limits (IDL) and estimated quantitation limits (EQL) shown are for acidified water and/or fusion flux matrices as applicable. Method detection limits (MDL) for individual samples can be estimated by multiplying the IDL by the "Process Factor" for that individual sample. The estimated quantitation limit (EQL) for each concentration value can be obtained by multiplying the EQL by the "Process Factor".
3) Routine precision and bias is typically ±15% or better for samples in dilute, acidified water (e.g. 5% v/v HNO_3 or less) at analyte concentrations > EQL up to the upper calibration level. This also presumes that the total dissolved solids concentration in the sample is less than 5000 µg/mL (0.5 per cent by weight). Note that bracketed values listed in the data report are within the MDL and the EQL, and have potential uncertainties greater than 15%. Concentration values < MDL are listed as "- -". Note, that calibration and QC standard samples are validated to a precision of ±10%.
4) Analytes included in the spike A component (for the AS/PS) are; Ag, Al, As, B, Ba, Be, Bi, Ca, Cd, Co, Cr, Cu, Eu, Fe, K, Li, Mg, Mn, Mo, Na, Ni, P, Pb, Sb, Se, Si, Sm, Sn, Sr, Ta, Ti, Tl, V, W, Y, Zn, and Zr. Analytes included in the spike B component are; Ce, Dy, Eu, La, Nd, Pd, Rh, Ru, S, Te, Th, and U.

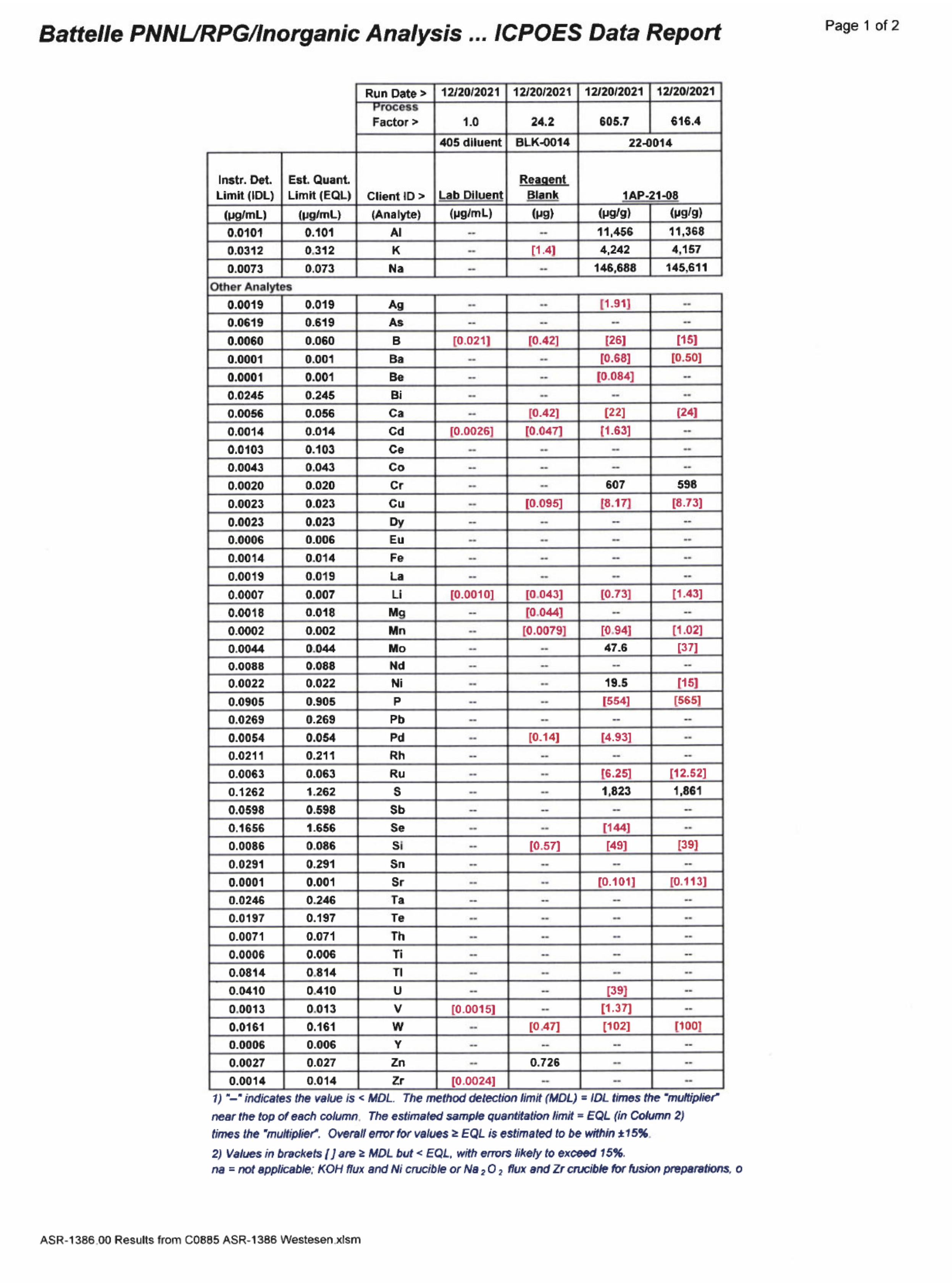

Battelle PNNL/RPG/Inorganic Analysis ... ICPOES Data Report

Page 1 of 2

		Run Date >	12/20/2021	12/20/2021	12/20/2021	12/20/2021
		Process Factor >	1.0	24.2	605.7	616.4
			405 diluent	BLK-0014	22-0014	
Instr. Det. Limit (IDL)	Est. Quant. Limit (EQL)	Client ID >	Lab Diluent	Reagent Blank	1AP-21-08	
(µg/mL)	(µg/mL)	(Analyte)	(µg/mL)	(µg)	(µg/g)	(µg/g)
0.0101	0.101	Al	--	--	11,456	11,368
0.0312	0.312	K	--	[1.4]	4,242	4,157
0.0073	0.073	Na	--	--	146,688	145,611
Other Analytes						
0.0019	0.019	Ag	--	--	[1.91]	--
0.0619	0.619	As	--	--	--	--
0.0060	0.060	B	[0.021]	[0.42]	[26]	[15]
0.0001	0.001	Ba	--	--	[0.68]	[0.50]
0.0001	0.001	Be	--	--	[0.084]	--
0.0245	0.245	Bi	--	--	--	--
0.0056	0.056	Ca	--	[0.42]	[22]	[24]
0.0014	0.014	Cd	[0.0026]	[0.047]	[1.63]	--
0.0103	0.103	Ce	--	--	--	--
0.0043	0.043	Co	--	--	--	--
0.0020	0.020	Cr	--	--	607	598
0.0023	0.023	Cu	--	[0.095]	[8.17]	[8.73]
0.0023	0.023	Dy	--	--	--	--
0.0006	0.006	Eu	--	--	--	--
0.0014	0.014	Fe	--	--	--	--
0.0019	0.019	La	--	--	--	--
0.0007	0.007	Li	[0.0010]	[0.043]	[0.73]	[1.43]
0.0018	0.018	Mg	--	[0.044]	--	--
0.0002	0.002	Mn	--	[0.0079]	[0.94]	[1.02]
0.0044	0.044	Mo	--	--	47.6	[37]
0.0088	0.088	Nd	--	--	--	--
0.0022	0.022	Ni	--	--	19.5	[15]
0.0905	0.905	P	--	--	[554]	[565]
0.0269	0.269	Pb	--	--	--	--
0.0054	0.054	Pd	--	[0.14]	[4.93]	--
0.0211	0.211	Rh	--	--	--	--
0.0063	0.063	Ru	--	--	[6.25]	[12.52]
0.1262	1.262	S	--	--	1,823	1,861
0.0598	0.598	Sb	--	--	--	--
0.1656	1.656	Se	--	--	[144]	--
0.0086	0.086	Si	--	[0.57]	[49]	[39]
0.0291	0.291	Sn	--	--	--	--
0.0001	0.001	Sr	--	--	[0.101]	[0.113]
0.0246	0.246	Ta	--	--	--	--
0.0197	0.197	Te	--	--	--	--
0.0071	0.071	Th	--	--	--	--
0.0006	0.006	Ti	--	--	--	--
0.0814	0.814	Tl	--	--	--	--
0.0410	0.410	U	--	--	[39]	--
0.0013	0.013	V	[0.0015]	--	[1.37]	--
0.0161	0.161	W	--	[0.47]	[102]	[100]
0.0006	0.006	Y	--	--	--	--
0.0027	0.027	Zn	--	0.726	--	--
0.0014	0.014	Zr	[0.0024]	--	--	--

1) "--" indicates the value is < MDL. The method detection limit (MDL) = IDL times the "multiplier" near the top of each column. The estimated sample quantitation limit = EQL (in Column 2) times the "multiplier". Overall error for values ≥ EQL is estimated to be within ±15%.

2) Values in brackets [ ] are ≥ MDL but < EQL, with errors likely to exceed 15%.

na = not applicable; KOH flux and Ni crucible or Na_2O_2 flux and Zr crucible for fusion preparations, o

ASR-1386.00 Results from C0885 ASR-1386 Westesen.xlsm

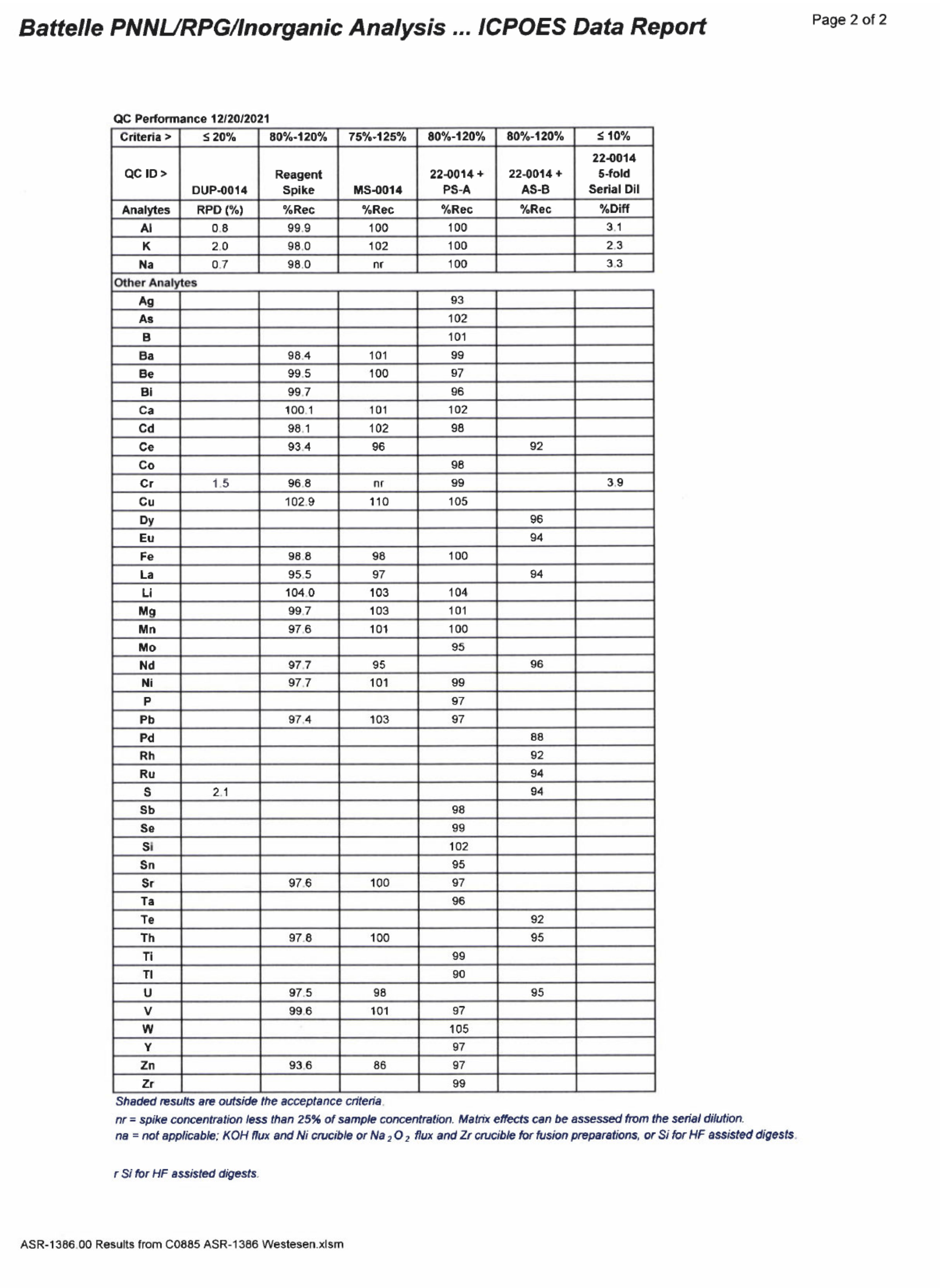

Battelle PNNL/RPG/Inorganic Analysis ... ICPOES Data Report

Page 2 of 2

QC Performance 12/20/2021

Criteria >	≤ 20%	80%-120%	75%-125%	80%-120%	80%-120%	≤ 10%
QC ID >	DUP-0014	Reagent Spike	MS-0014	22-0014 + PS-A	22-0014 + AS-B	22-0014 5-fold Serial Dil
Analytes	RPD (%)	%Rec	%Rec	%Rec	%Rec	%Diff
Al	0.8	99.9	100	100		3.1
K	2.0	98.0	102	100		2.3
Na	0.7	98.0	nr	100		3.3
Other Analytes						
Ag				93		
As				102		
B				101		
Ba		98.4	101	99		
Be		99.5	100	97		
Bi		99.7		96		
Ca		100.1	101	102		
Cd		98.1	102	98		
Ce		93.4	96		92	
Co				98		
Cr	1.5	96.8	nr	99		3.9
Cu		102.9	110	105		
Dy					96	
Eu					94	
Fe		98.8	98	100		
La		95.5	97		94	
Li		104.0	103	104		
Mg		99.7	103	101		
Mn		97.6	101	100		
Mo				95		
Nd		97.7	95		96	
Ni		97.7	101	99		
P				97		
Pb		97.4	103	97		
Pd					88	
Rh					92	
Ru					94	
S	2.1				94	
Sb				98		
Se				99		
Si				102		
Sn				95		
Sr		97.6	100	97		
Ta				96		
Te					92	
Th		97.8	100		95	
Ti				99		
Tl				90		
U		97.5	98		95	
V		99.6	101	97		
W				105		
Y				97		
Zn		93.6	86	97		
Zr				99		

Shaded results are outside the acceptance criteria.

nr = spike concentration less than 25% of sample concentration. Matrix effects can be assessed from the serial dilution.

na = not applicable; KOH flux and Ni crucible or Na_2O_2 flux and Zr crucible for fusion preparations, or Si for HF assisted digests.

r Si for HF assisted digests.

ASR-1386.00 Results from C0885 ASR-1386 Westesen.xlsm

Appendix E – Backpulse AP-101 Characterization with Scanning Electron Microscopy Coupled with Automated Particle Analysis

E.1 Microscopy Methods

Materials from Hanford tank waste derived material, AP-101 supernatant, were examined with scanning electron microscopy (SEM) and with higher resolution scanning transmission electron microscopy (STEM). Two samples were provided for microscopy analysis: (1) a liquid and (2) the dried crystallized particles from the supernatant (see Figure E.1). Supernatant samples from AP-101 were reported to have concentrations approaching 8.89 M Na and 3.0 M NO_3, so we would expect the sample to be dominated by crystallized sodium nitrate phases (Esch 1996; Fiskum et al. 2000). Samples for microscopy analyses from the supernatant were prepared using methods to avoid the formation of evaporative salts as much as possible, in order to locate suspended insoluble particles. Analysis of the solids was dominated by the salt components.

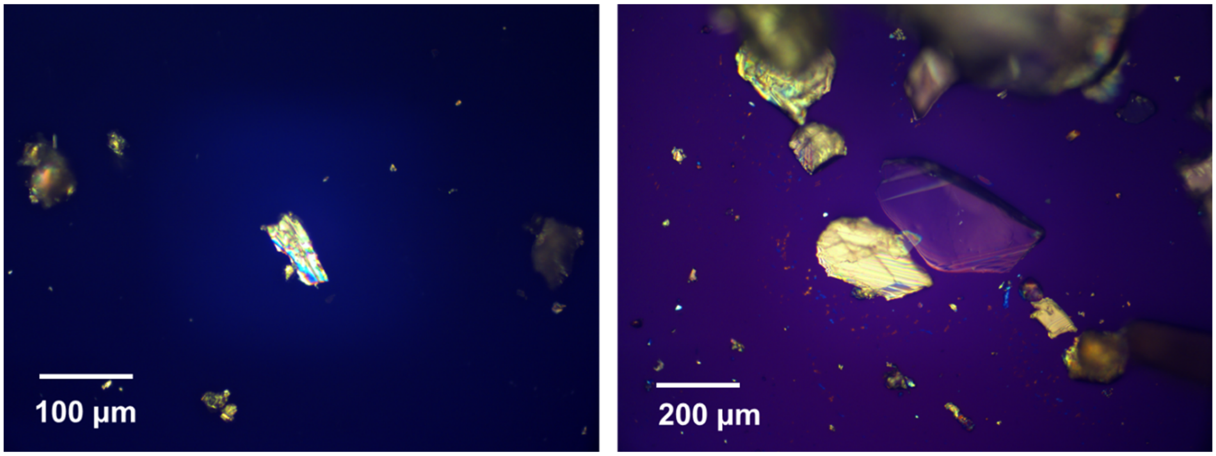

Figure E.1. Cross-polar polarized light microscope images of AP-101 supernatant-solids sample taken at ×100 (A) and ×200 (B) from the "as-received" solids. Many of the particles were large chunks that had to be broken down as they had stuck to the bottom of the collection vial.

Initial observations on the samples were conducted with optical microscopy using a Nikon 400POL polarized light microscope equipped with a Lumera digital camera. Length scale was calibrated with a National Institute of Standards and Technology Standard Reference Material 2800, Microscope Magnification Standard.

The samples were further examined with an FEI (Thermo-Fisher Inc., Hillsboro, OR) Quanta 250 field emission gun equipped with secondary electron (SE) and backscattered electron (BSE) detectors, and EDAX (EDAX Inc., NJ) Genesis X-ray energy dispersive spectroscopy (EDS) system. No conductive carbon coat was used on the sample, requiring the instrument to be operated in the low-vacuum mode on occasions.

To prepare the sample from the liquid sample and avoid formation of salts and evaporites, the sample was pipetted onto a transmission electron microscopy (TEM) grid with a holey carbon film. The film acted as a filter for the particles, allowing most of the solution to wick through. The grid was then applied to a SEM sticky-carbon stub to attach the particles (see Figure E.1B). This technique sometimes resulted in some copper micro-particles in the sample. With the solid sample, materials were removed directly from the vial and deposited onto an SEM stub. The stub was aluminum with a sticky carbon film for capturing the particles. The solid particles in the vial had cemented together and adhered tenaciously to the glass, and it required some effort to remove material.

As in previous campaigns, the particles obtained from the waste treatment process or from Hanford particle characterization campaigns (Buck and McNamara 2004; Cantrell et al. 2014; Krupka 2006; Lumetta et al. 2009) were analyzed in a manual mode, in which the analyst located particles with unique forms or contrast, placed the electron beam on the particle, and collected an EDS spectrum. Identification of a specific phase was based on post-examination of the image and spectral data. This type of manual analysis is accurate but is relatively laborious and time consuming (Brożek-Mucha 2014; Laskin and Cowin 2001). In this investigation, the analysis process was automated, enabling information to be provided on thousands of particles. The phases were grouped according to the EDS composition and assigned a classification by the operator. The data was exported to a Jupyter Notebook for analysis. Data was plotted with the aid of the Python packages matplotlib and pyrolite (https://pyrolite.readthedocs.io/en/main/).

The object of automated analysis is to remove potential operator bias from the analysis and to yield statistically useful data. Previous studies have shown the potential for this method to improve the quality of SEM analyses; however, the results do depend on consistent sample preparation methods.

The material from the liquid sample was further examined with STEM using a JEOL (JEOL Inc., Japan) ARM300F (GrandARM) microscope. Samples were prepared by pipetting the radioactive solution onto a TEM grid. Any large particles had to be removed manually from the TEM grid. STEM images were collected using an annular dark field detector and compositional analysis was obtained with EDS. Samples were also analyzed under TEM mode, enabling selected area electron diffraction (SAED) patterns to be collected. The diffraction patterns were analyzed with DigitalMicrograph™ 3.0 software and utilizing scripts developed by Mitchell (2008).

E.2 Microscopy Solids Analysis

In contrast to previous recent analyses of solids from filtration experiments, the overall composition and variability in the solids was limited. Most of the material had crystallized into large particles that had to be broken up prior to imaging in the microscopes. Therefore, the size of any particles or agglomerates was dependent on how the sample was prepared. Particles larger than 200 to 500 µm were not uncommon (see Figure E.1 and Figure E.2). However, particle size analysis was performed on the data (see Figure E.5). Samples extracted from the solid sample had to be broken up prior to transferring them to a SEM stub, and the liquid sample resulted in the rapid precipitation of the material if the solution was not wicked away quickly enough and washed with an alcohol. The SEM analysis revealed that particles were mainly a sodium-nitrogen compound. Many of the particles were too large for normal SEM analysis as they exceeded 1-mm in size (see Figure E.2). Manual SEM analysis, automated analysis, and STEM investigations were all employed in this study. A series of images of the material were collected with BSE imaging, and EDS mapping and spot analysis was performed to gain an understanding of the types of phases present in the material (see Figure E.2 for examples of the morphologies in the specimen).

Automated particle analysis with SEM-EDS failed to indicate the presence of sulfur or phosphorus bearing phases in the specimen. These elements are common in many of the phases observed in the Hanford tanks and can often precipitate extremely rapidly from solution. However, elemental mapping did suggest the presence of fluorine in many particles. Many of the fluorine containing phases reported in the Hanford tanks have also been shown to contain sulfur, such as Na_3FSO_4. Fluorine maps are shown from the SEM results; however, during automated particle analysis, this element was listed. We will show later that fluorine was unlikely to be present at the levels indicated by the maps as this element could not be located with STEM-EDS in later investigations. One reason for the discrepancy is that the SEM-EDS system has a lower or poorer energy resolution than the system used on the STEM. The major elements detected included carbon, oxygen, nitrogen, and sodium. Aluminum and silicon bearing phases were also observed. Very few heavy elements were observed. Possible phases that could include these combinations of elements and have been found in the Hanford tank wastes, including $Na_2C_2O_4$, $Na_2CO_3•H_2O$, $NaNO_3$, and $NaNO_2$. Aluminum and silicon phases have been reported as cancrinite or nitrate-cancrinite, amongst other phases.

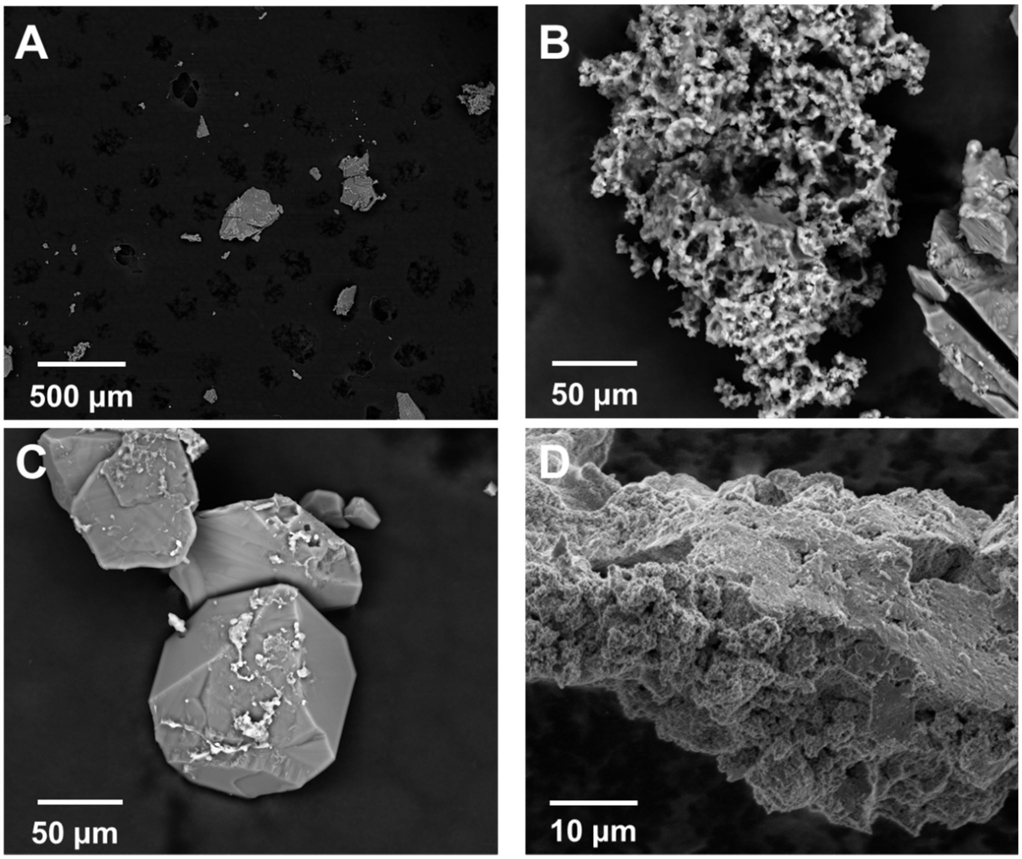

Figure E.2. SEM images of example morphologies observed in AP-101 supernatant: (A) distribution of particles taken a low magnification; (B) high surface area agglomerate particle containing Al; (C) angular block particles with high Z material attached to the surface; (D) high magnification view of particle. Some particles were very large, almost 1 mm long crystal with a block-like appearance similar to that from $NaNO_3$.

Sodium oxalate ($Na_2C_2O_4$) is known to occur as small rods or prisms, but in tank wastes has been most often observed as acicular crystals (Wells et al. 2011). Sodium carbonate is also commonly found in the waste tanks and often has blade-like edges (Herting and Cooke 2002).

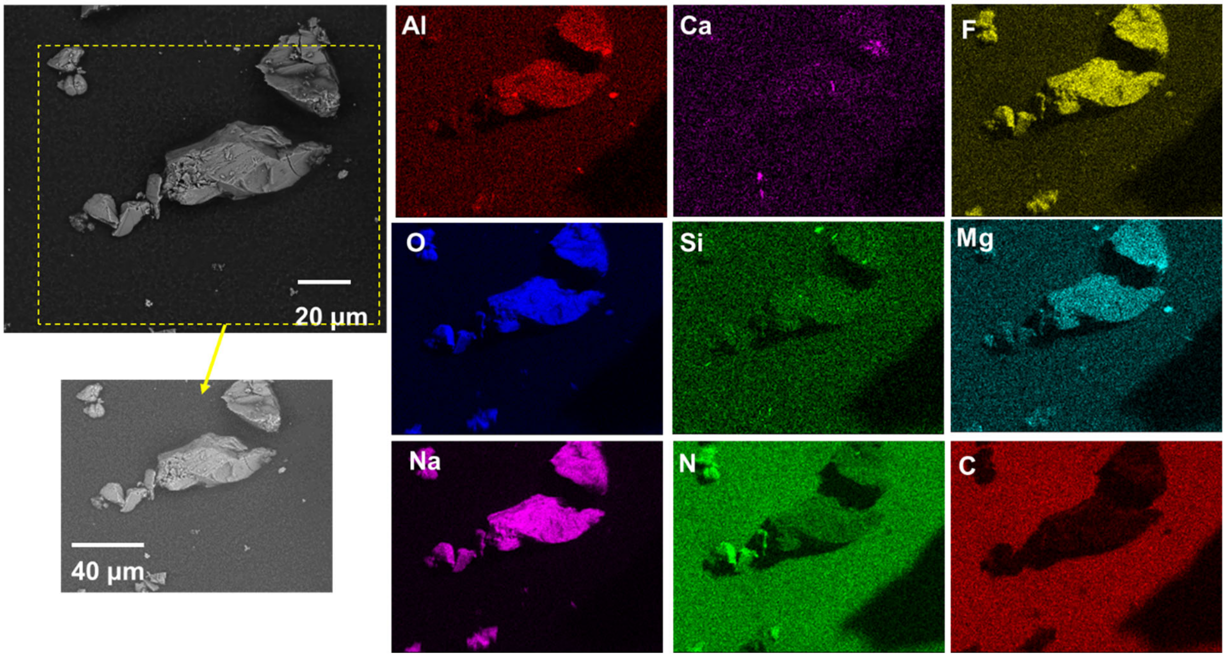

Figure E.3. SEM-EDS elemental maps of the large particles found in the concentrate showing sodium-rich, aluminum-particles. The yellow outline in the SE image is the same region in Figure E.2B and shows that this large particle is most likely sodium nitrate.

The detection of carbon with SEM-EDS is problematic because the support film is carbon. The results do not support the presence of a carbon containing phase in most of the elemental maps. The SEM image and elemental maps in Figure E.3 revealed several phases, including a sodium nitrate, calcite-like phase, and aluminum oxides. The fluorine map is supportive of a high fluorine containing phase; however, we will show later that this is likely an artifact. Both sulfur and phosphorus were present in the supernatant at 0.0411 M and 0.0129 M, respectively. However, phases containing these elements were not readily identified during elemental mapping. Correlative plots do, however, show a relationship between these two elements (see Figure E.8). SEM-EDS of several different phases is shown in Figure E.4. Initial investigations detected copper, but these could have been artifacts from the TEM grid from sample preparation, although copper was present in the supernatant at 8.17 µg/g. In contrast, both chromium and nickel were present in the supernatant at higher concentrations (see Figure E.6B). Observations of these phases are discussed later.

As further improved preparations of the supernatant and solids were made, the copper artifact was eliminated. In Figure E.5, the size distribution of many particles from prepared samples is shown. The plots show the distribution of particles according to their average diameter and their area. The area plot is a log-normal plot that has been fitted to a Gaussian.

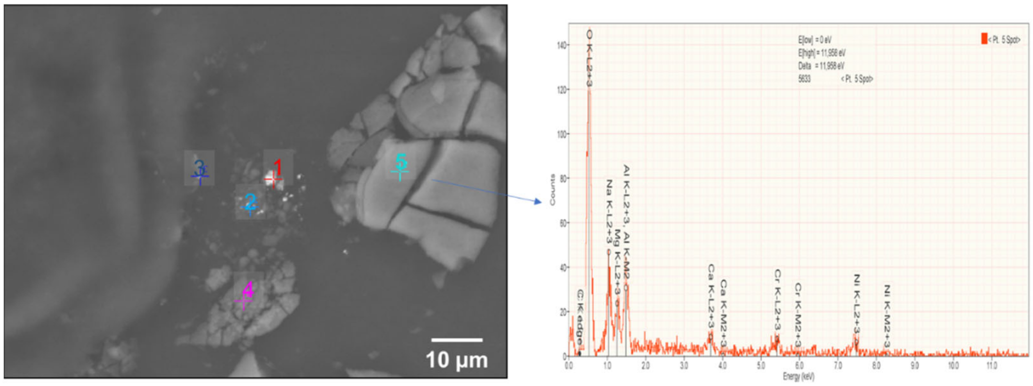

Figure E.4. SEM image and EDS spectrum of a selected particle in AP-101 supernatant. The locations indicate analysis points referenced in Table E.1.

Using automated particle analysis, a series of compositional ternary diagrams were developed (see Figure E.6) for some major elements to provide an overview of the compositions in the material (see Table E.1). Compositional plots are more useful than the particle morphology information in this case. Particle size and shape varied depending on how the material was prepared for analysis.

The particle sizes closely approximated a log-normal distribution, which is typical for most particles (see Figure E.5). In Figure E.6A and B and Figure E.8A, compositional ternary diagrams show evidence for common compositions through the clustering of data values. The scatter diagrams in Figure E.7 show that the different distributions of Fe and Na are both associated with similar distributions of particle sizes.

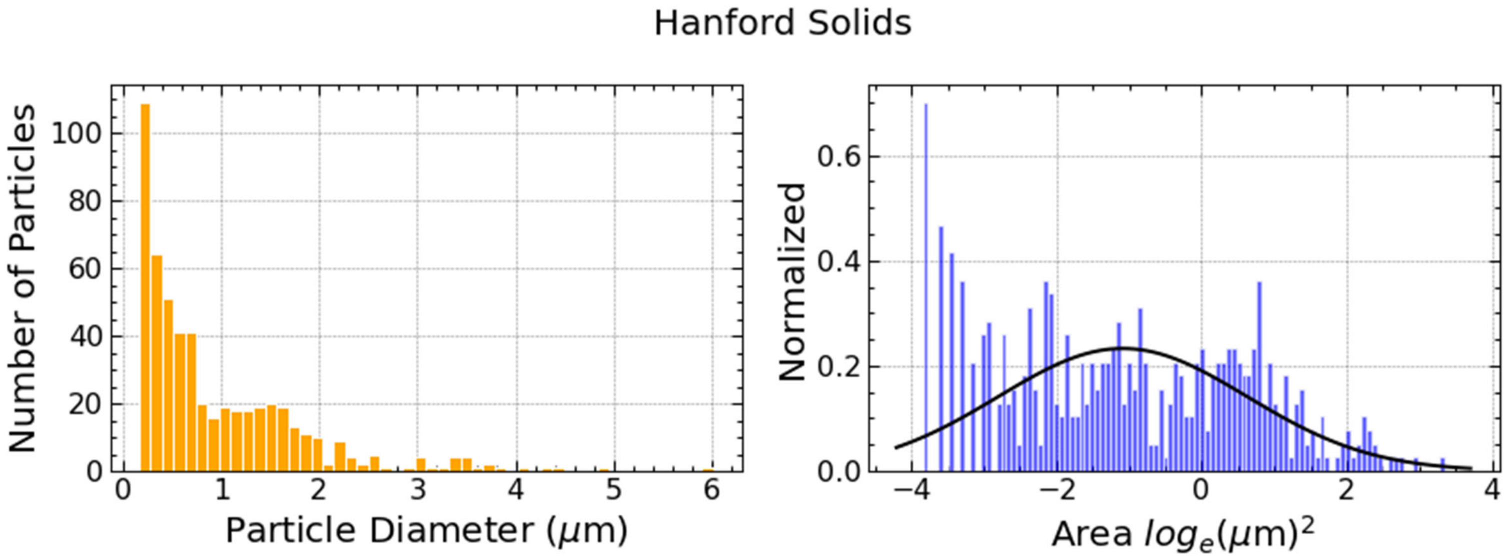

Figure E.5. Particle size analysis from AP-101 supernatant-solids. The yellow histogram shows the average particle diameter. Very large particles were excluded. The blue histogram describes the area of these particles in a log-normal plot.

Table E.1. Particle compositions from a selected number of phases as shown in Figure E.4 (element wt%).

Location	CK	NK	OK	NaK	MgK	AlK	SiK	AgL	CaK	TiK	CrK	FeK	NiK	CuK
1	10.71	5.03	36.68	6.64	3.36	8.66	1.82	21.38	0.63	0.71	0.67	1.56	1.18	0.98
2	20.89	10.81	40.25	6.19	2.91	7.22	1.72	3.86	0.71	1.22	1.05	0.73	1.22	1.22
3	23.01	14.16	38.77	3.83	2.93	4.98	2.46	3.41	1.11	1.27	0.85	1.33	0.79	1.11
4	7.24	2.86	52.4	27.73	1.66	4.61	0.22	0.73	0.6	0.1	0.73	0	1.11	0
5	0	0	51.68	16.03	9.19	12.84	0.76	1.18	2.07	0	1.88	0.49	3.88	0

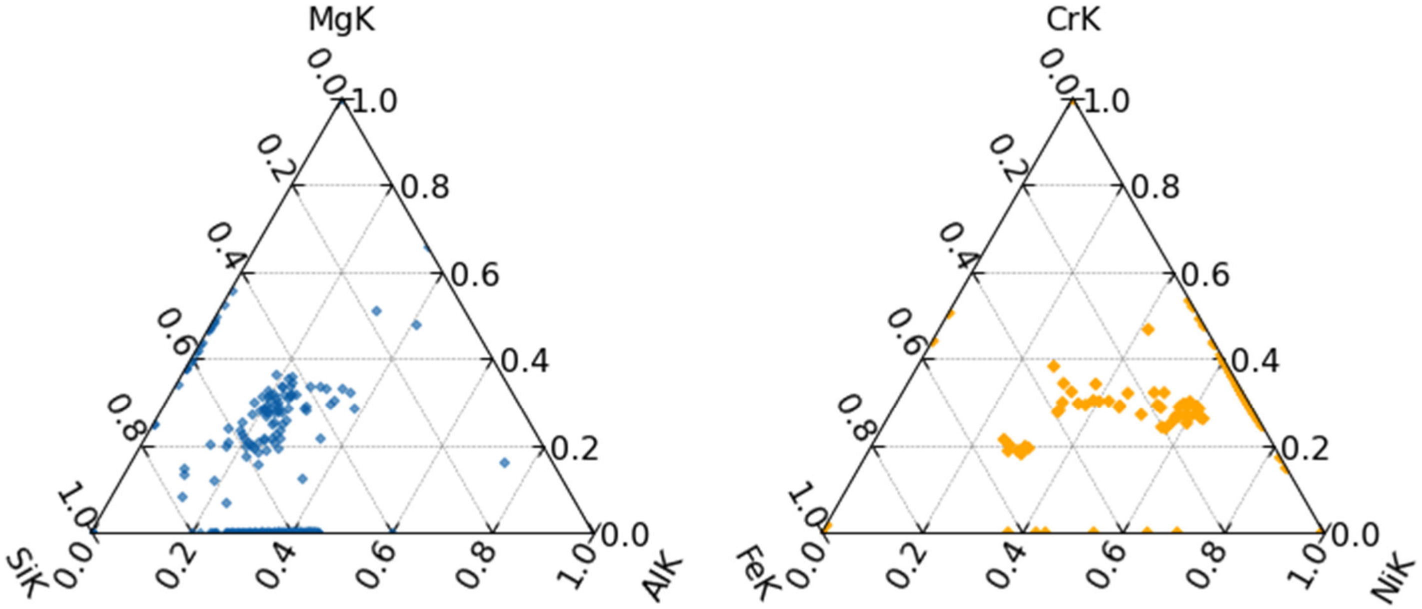

Figure E.6. Ternary plots of selected elements in AP-101 supernatant-solids for major phases (A) and the first-row transition elements (B), both with well-defined composition bounds, suggesting a specific phase is present.

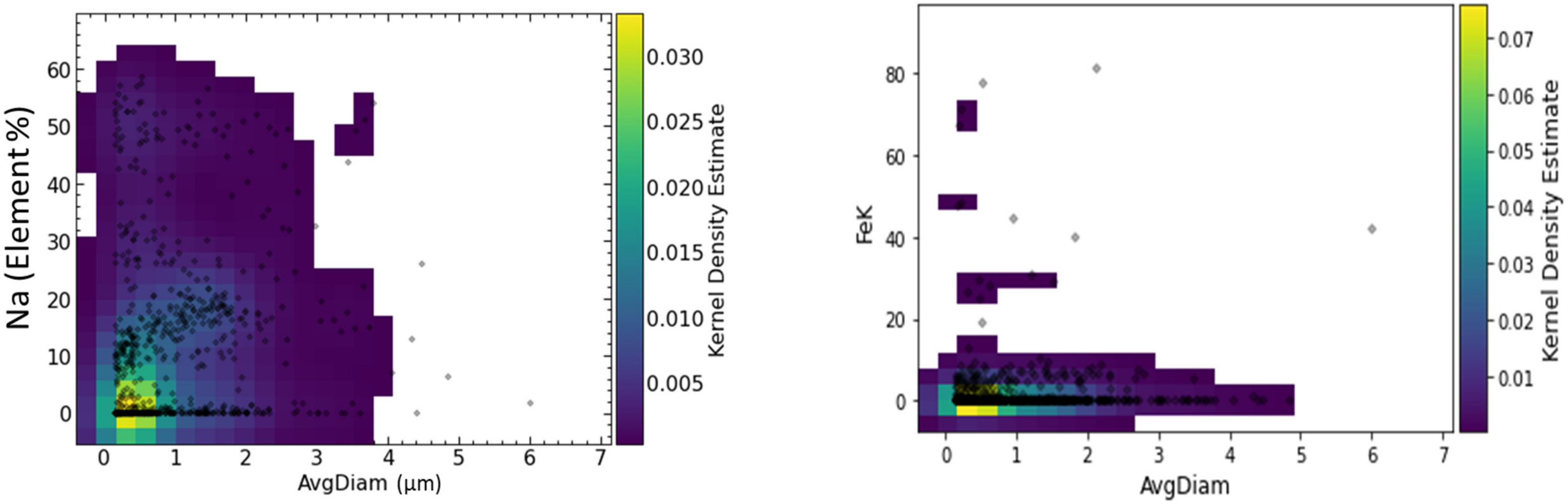

Figure E.7. Major types of sodium phases with average particle size for (A) sodium and (B) iron. The plots show both the distribution of data and individual data points that show how far at times individual results deviate from the average.

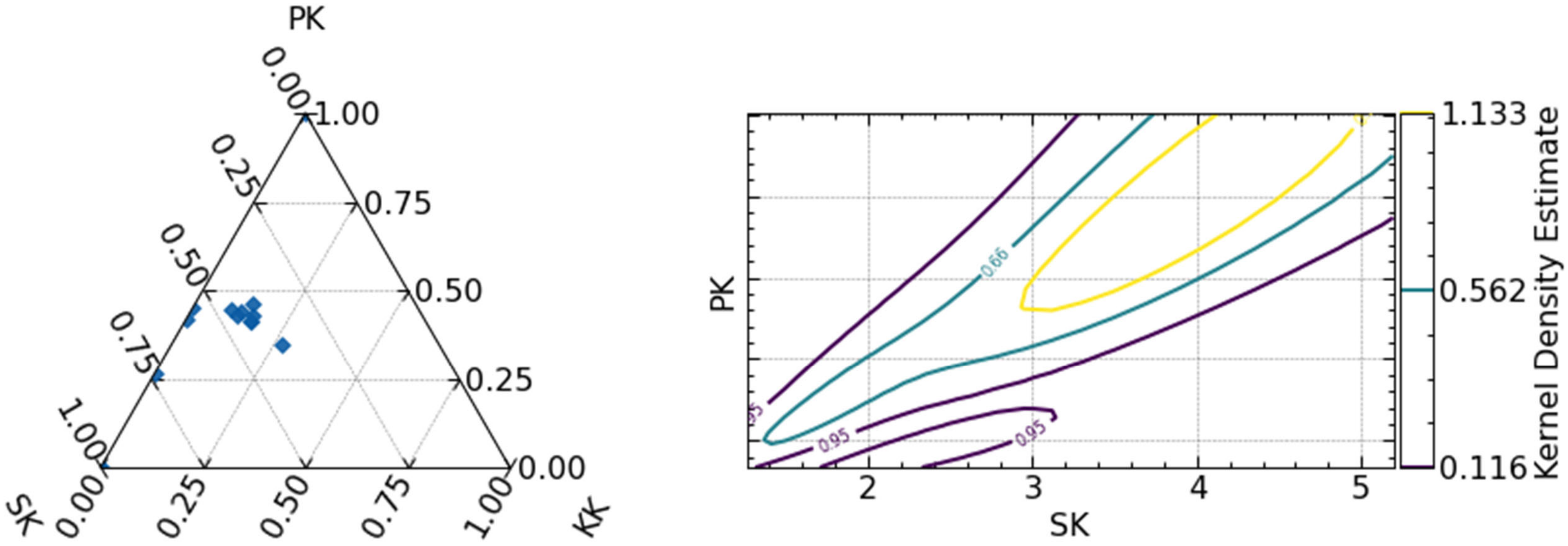

Figure E.8. Apparent association of sulfur and phosphorus in the AP-101 supernatant in (A) ternary plot and (B) correlation plot.

Occurrence of an aluminosilicate phase

Figure E.9 shows SEM-EDS analysis of an aluminum oxide phase. The particles appeared to be round particles. This morphology was consistent with cancrinite-type zeolitic phases that are known to occur in Hanford tank wastes. These phases may exist as colloids in the supernatant as they would be unlikely to form rapid precipitation from solution, unlike the sodium nitrate crystals.

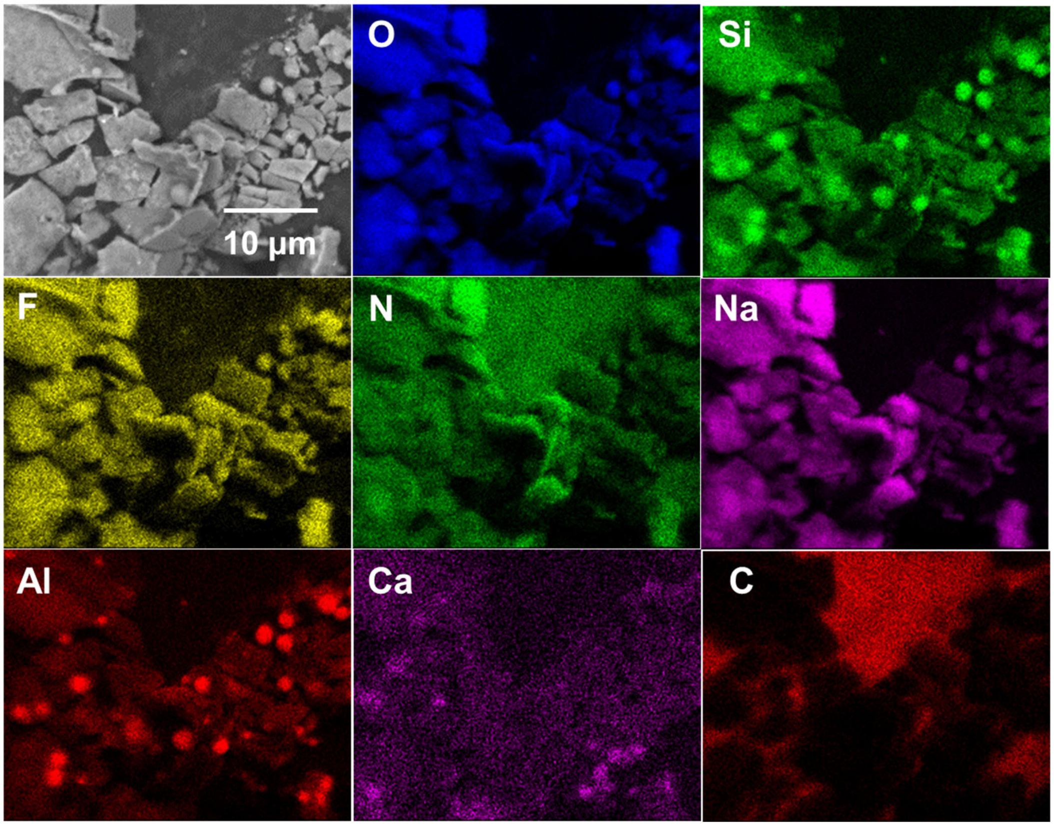

Figure E.9. Elemental map of particle agglomerate from AP-101 supernatant-solids. The elemental maps show the presence of a round aluminosilicate phase on the surface of a sodium nitrate material. The maps of fluorine and nitrogen are questionable. The aluminosilicate particles were < 1 µm in diameter..

These particles were found in other areas, and several maps show the existence of these phases in the supernatant sample. Figure E.10 shows another example of these small particles. They were not visible during the initial imaging and were only revealed following a long elemental map collection. There is also evidence of two other phases: (1) a Ca-Mg phase, which may also contain Si and Al, and (2) a Mg-silicate phase. However, the entire agglomerate is dominated by the presence of the sodium nitrate phase.

The SEM-EDS results showed the limited number of particle types in the specimen. The major phase identified appeared to be nitrate and sodium oxalate. The large crystals that formed could be observed readily with the naked eye, under the polarized light microscope, and in the SEM. In Figure E.11, another example of these phases can be seen. The block-like phase is sodium nitrate. The occurrence of fluorine was of interest as is whether carbon-containing phases were present. However, because of its poor resolution, the EDS system on the SEM may not be completely reliable for the analysis of fluorine, and the use of sticky carbon surfaces for SEM prevents analysis of carbon in any phases. This was one reason to perform STEM analysis with its superior analytical capabilities.

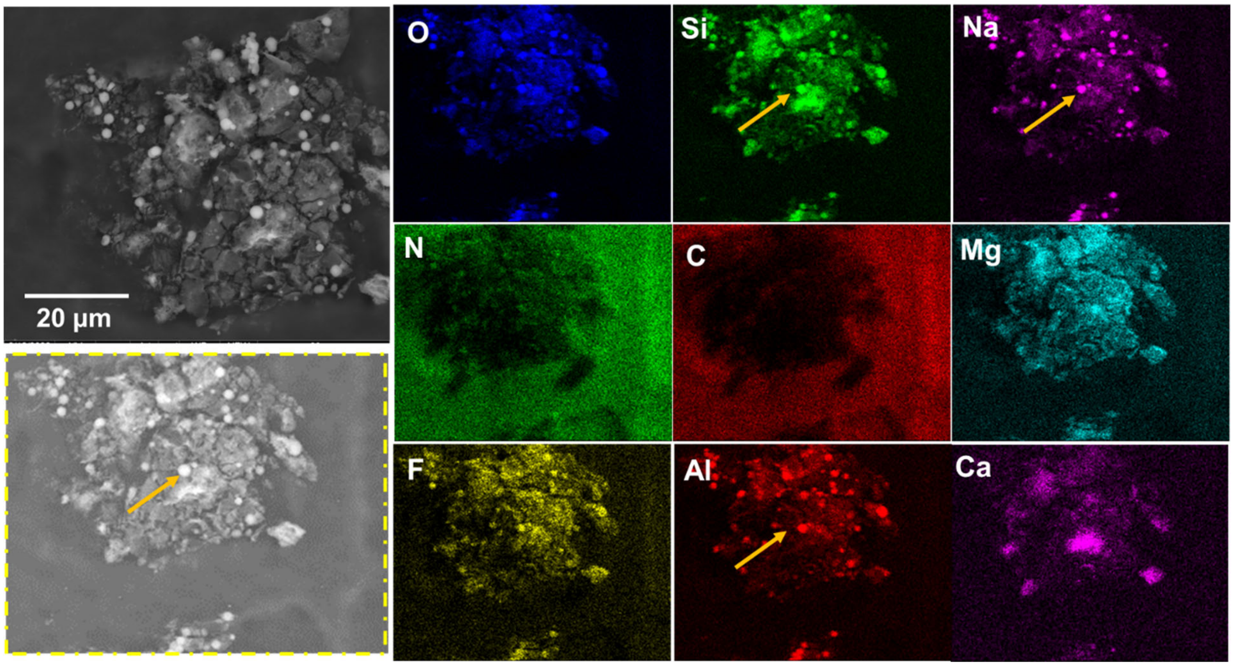

Figure E.10. BSE images and elemental maps of a particle agglomerate from AP-101 supernatant-solids. The elemental maps show the presence of a round aluminosilicate phase (indicated by arrow).

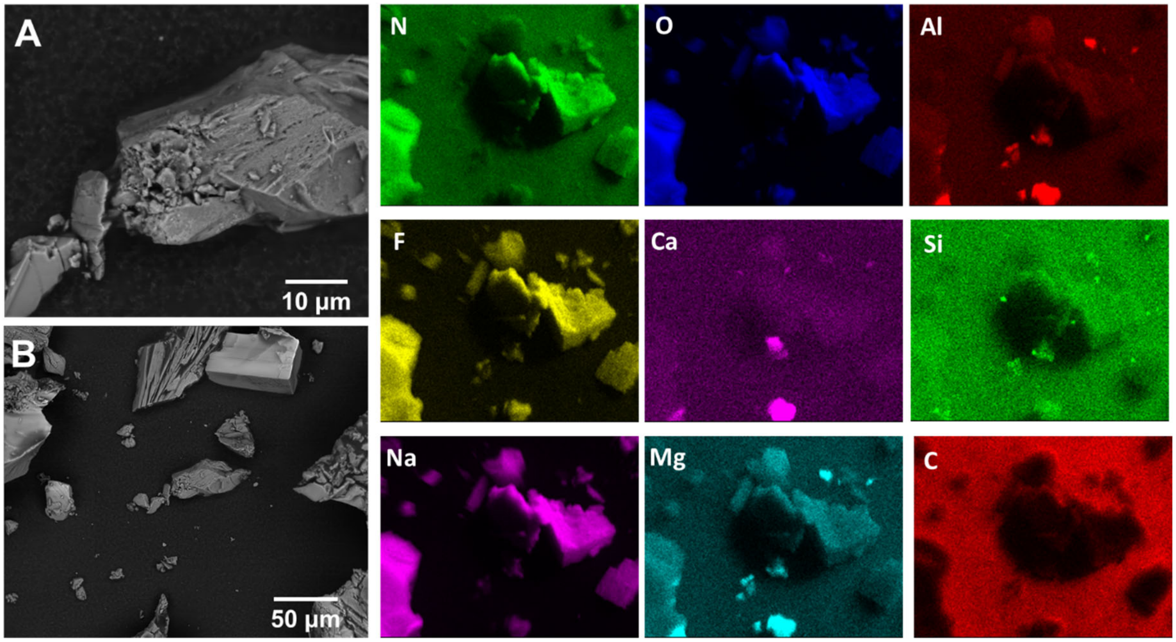

Figure E.11. Images and elemental maps (taken from nearby region) of block-shaped sodium nitrate particles from AP-101 supernatant-solids. The elemental maps show the presence of a round Ca-Al-Mg phase. The maps of fluorine and nitrogen are questionable and needed confirmation with STEM analysis.

Herting and Cooke (2002; see Figure 7-16, p. 82) observed round Na-aluminosilicates compositionally and morphologically similar to the particles found in this study; although the particles found in AP-101 supernatant are about a tenth the size of the ones reported in tank 241-C-108. Buck and McNamara (2004) also observed the formation of a cancrinite in a sludge sample from AP-101; however, again these were much larger particles than observed in this case. If these aluminosilicates are suspended in the supernatant, they would be expected to have colloidal dimensions. The particles shown in the elemental maps above do have the dimensions of colloids. They have, however, sorbed to the surfaces of precipitating sodium nitrate particles during the sample preparation process.

E.3 STEM-HAADF Analysis

STEM analysis was used to understand the nature of the non-sodium-bearing salt precipitates in the specimen, particularly the aluminosilicate that was identified in the SEM-EDS elemental maps; however, sodium-bearing salts were still common in the prepared samples and interfered with the analysis. In Figure E.12, STEM-EDS, which has a better spatial and energy resolution than the SEM system, shows that nitrogen is clearly visible in the particles. The high-angle annular dark-field (HAADF) image and elemental maps show the sodium phases but there are also other phases, notably aluminosilicate particles. Na-C-O phases, Na-O-N phases, and Ca-O compositions were visible. This is a good indication that these phases formed during the sample preparation process. Other STEM-EDS analyses (see Figure E.14) highlighted an aluminosilicate particle. In contrast to the sodium-bearing phases, these particles were clearly crystalline and likely had been present in the suspended solids in the original AP-101 supernatant sample.

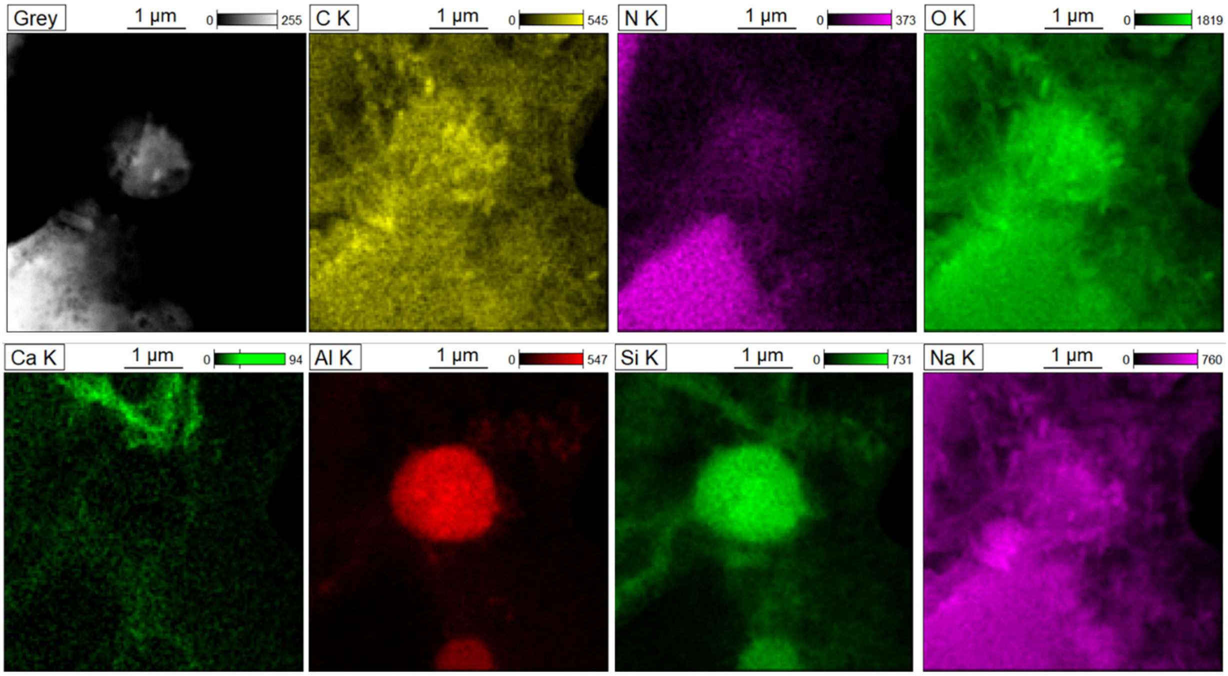

Figure E.12. Round aluminosilicate particles in the AP-101 supernatant sample. In this instance, the particle is hidden from view in the STEM-HAADF image, but the outline of the particle is revealed in the EDS mapping lying surrounded by a C-N-O film.

Excluding the dominant sodium nitrate material from the solids washing process, there appear to be Al-silicates, mixed Cr-Al oxide, and Fe-oxides phases. Within these phases, localized enrichment of Mg and Ca was only partly visible. These compositions could be consistent with phases previously identified in tank wastes, such as cancrinite and Fe-oxides. STEM-EDS and electron diffraction were used to investigate whether these phases could be present in the sample. Figure E.13 shows the occurrence of another colloidal-sized particle. This particle was identified as TiO_2 and is possibly a contaminant as there is no indication of Ti being present in the wastes. Figure E.14 is another example of the aluminosilicate phase and even though the particle is very thick, a weak electron diffraction pattern was obtained. The composition of the phase appears to be Na-O-Si-Al, which is entirely consistent with cancrinite. The electron diffraction results are reported in Table E.2 and are supportive of cancrinite being the phase present.

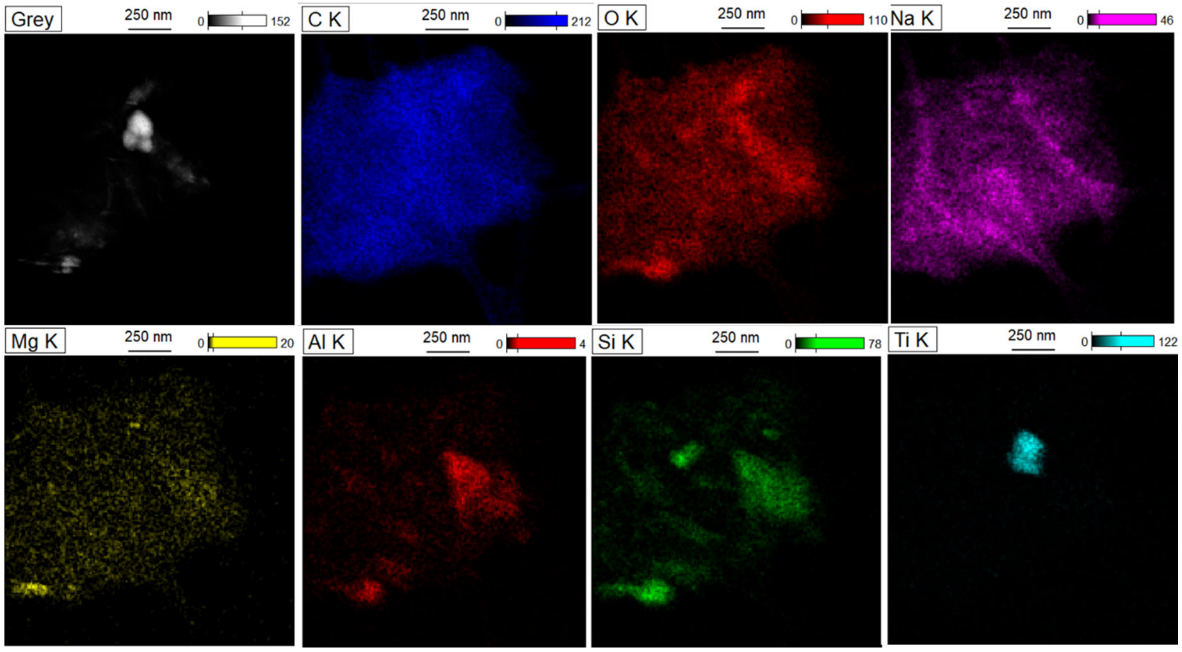

Figure E.13. Titanium oxide particle contained with other particles, notably a C-O-Na phase and separate Al-Si phase, and a Mg-Si-Al phase.

The SEM analysis and SEM-EDS analysis suggested very minor variation in compositions in the AP-101 supernatant sample. With STEM and its analytical capabilities, it was possible to make a more detailed investigation of the occurrence of any minor phases, if present, and to see if these could be described in greater detail. Ti and Mg phases were detected in the STEM-EDS analysis. As mentioned earlier, the Ti particle, which is found very easily because of its high contrast, is likely to be an artifact.

TEM and SAED were used to analyze a few of the phases observed. Figure E.15 shows TEM images of various different morphologies of particles observed in the AP-101 supernatant sample. None of the solids had a definitive crystalline morphology. Most seemed to be present as amorphous agglomerates. However, some diffraction patterns were obtained on these particles.

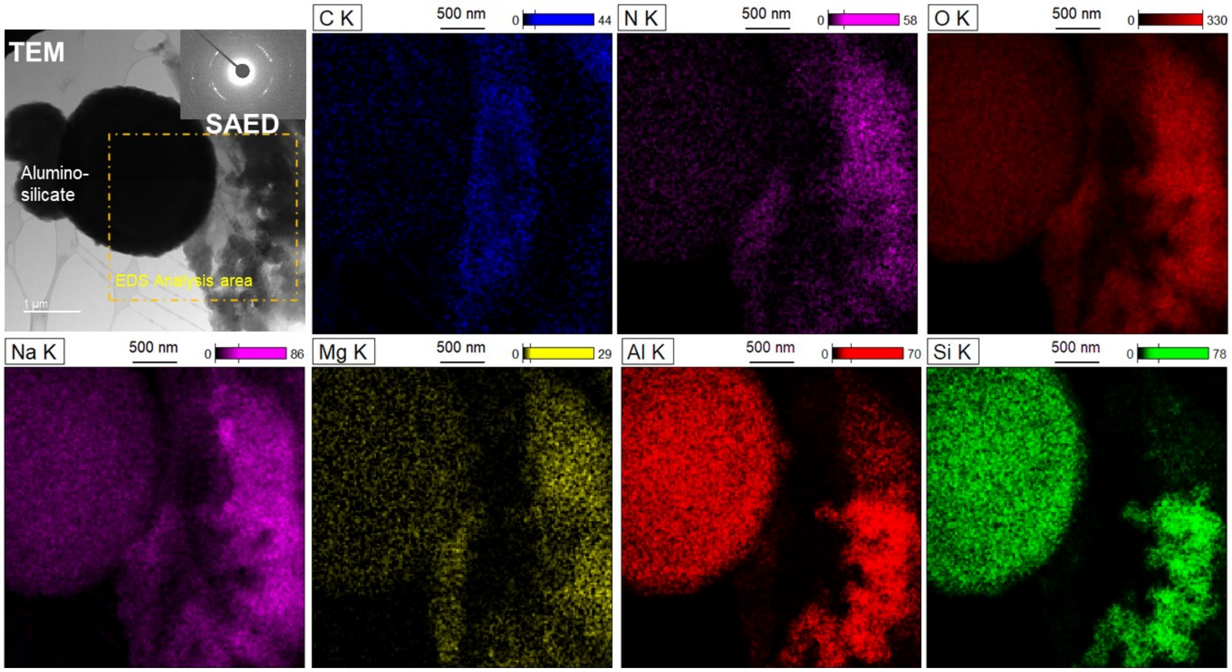

Figure E.14. TEM image of round particle found in AP-101 supernatant and STEM-EDS analysis of particle and neighboring areas. The round particle is an aluminosilicate. The remaining region to the right side appears to be nitrate.

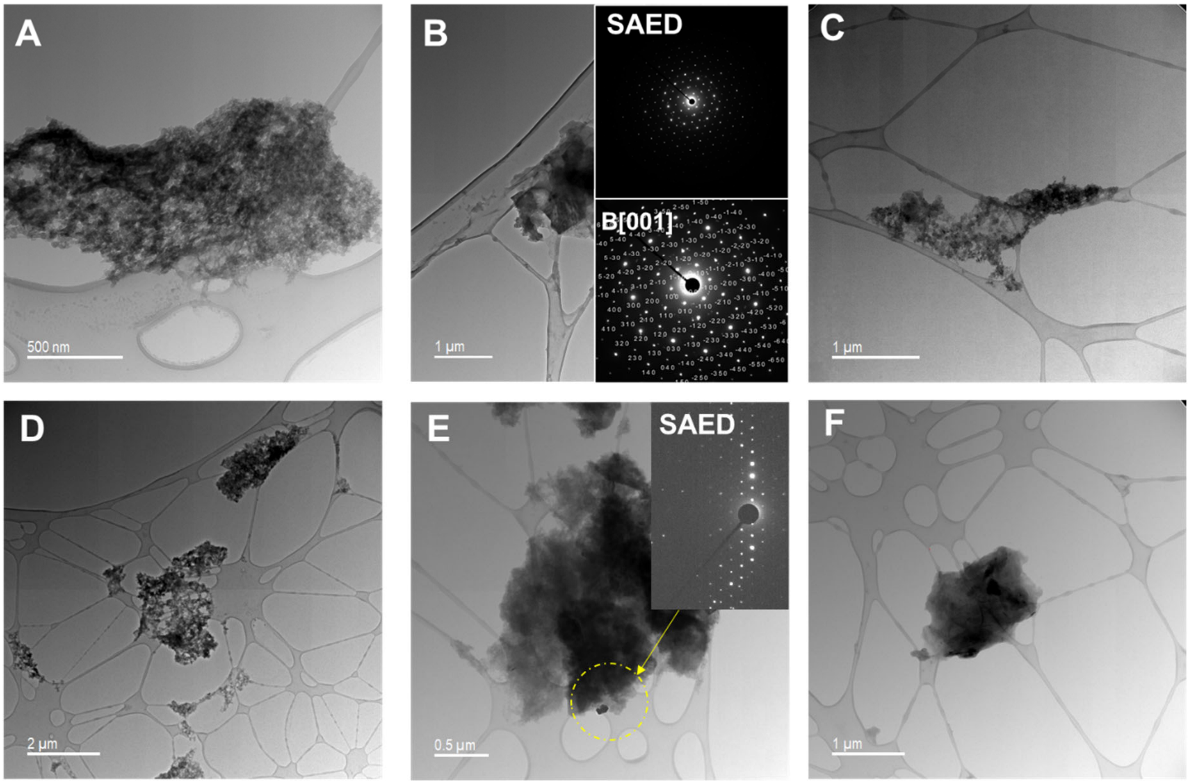

Figure E.15. (A-F) TEM images of particle agglomerates and insert SAED analyses (B and E). Using CrysTBox software, the SAED from particle in B was identified a pattern of $NaNO_3$ taken along the B[001] zone axis.

Table E.2. Electron diffraction analysis of the Al-Si particles.

Alumino silicate, (d/nm)	Nitrate Cancrinite, (d/nm)
	0.63353
	0.46906
	0.41483
	0.36589
0.319	0.32393
0.279	0.27439
	0.23328
0.200	0.21166
	0.20215
0.1549	0.15938
	0.15842
	0.14615

A weak ring pattern was obtained from the aluminosilicate phase and analyzed with scripts from Mitchell (2008). The spacings are listed in Table E.2 and were a good match to cancrinite. Additional electron diffraction results were obtained from phases from the TEM analysis and were analyzed with CrysTBox (Crystallographic Tool Box) software which uses computer vision analysis with comparisons to possible structures. The zone axe belonging to the solutions best fitting the experimental SAED data was shown to be the B[001] direction from sodium nitrate ($NaNO_3$).

E.4 Dissolution Investigations

Figure E.16 shows SEM-EDS elemental maps of the as-received solids. Several micron-sized particles can be seen. SEM-EDS elemental maps from the same region following dissolution are shown in Figure E.17. The background carbon film can be seen clearly in the elemental map for carbon. As dissolution proceeds, this area becomes covered with salt debris. There are at least two major compositionally different regions in the as-received analysis. Sodium dominates the area, but we can see that the left-hand side has an Al-Si phase present. Fluorine is again indicated, but as stated previously, there was no clear evidence of fluorine in that analysis.

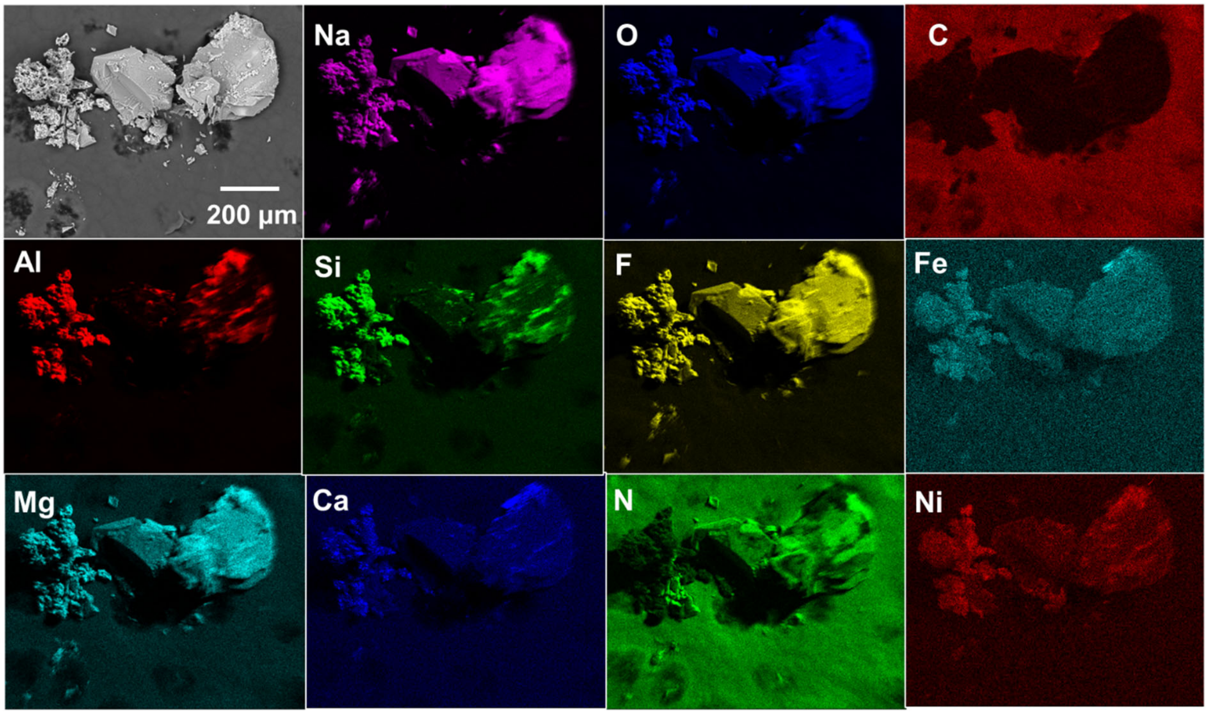

Figure E.16. SEM elemental map of AP-101 supernatant-solids particles prior to exposure to water vapor showing an Al-Si phase and sodium nitrate as the major phases.

The solids were partially dissolved in water to show that the majority of the material was readily soluble. To see the effect of this method on the specimen, a few experiments were performed exposing the prepared SEM sample to this solution. A cap containing a few drops of water was placed over the top of the SEM mount, creating a chamber where the sample was exposed to vapor. The intention was not to dissolve the particle directly but merely to look at partial dissolution. Figure E.17 shows the result of this partial dissolution on a sodium nitrate phase. The image shows extensive pitting and dissolution. A few smaller particles have been revealed through the dissolution process. It is not clear from the elemental analysis what these bright specks are composed of. However, none of the particles appeared to be unaffected by this process.

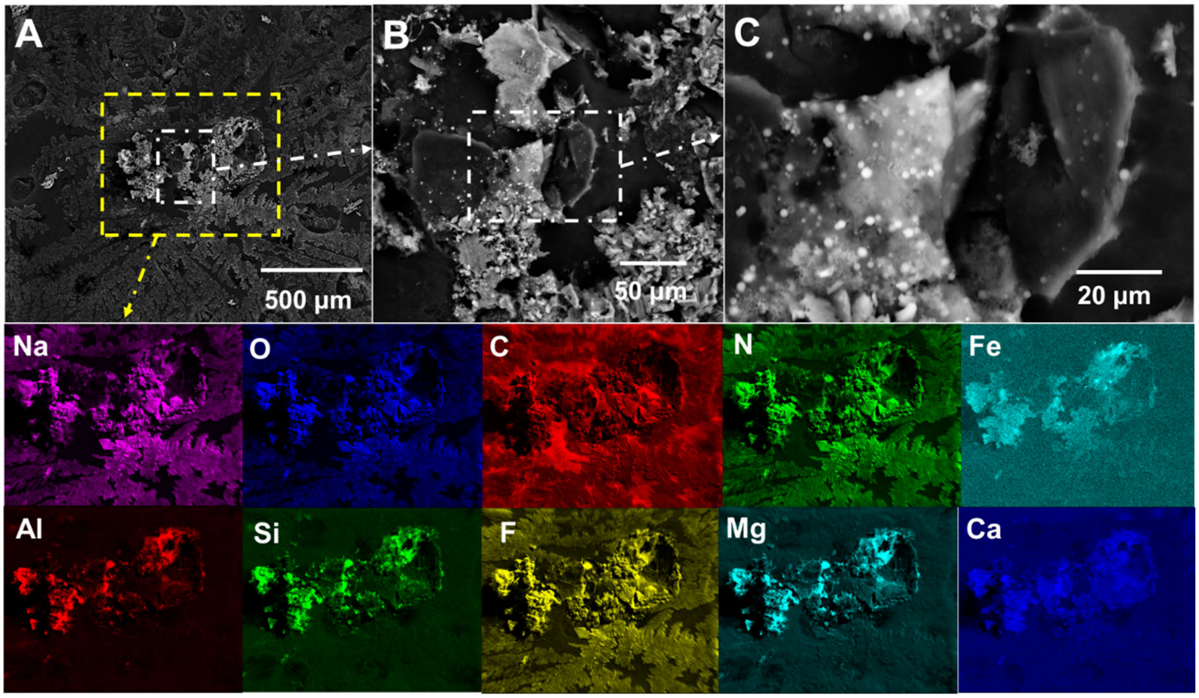

Figure E.17. Elemental map of AP-101 supernatant from the same area as in Figure E.15, exposed to water vapor for several hours, showing dissolution of salt phases and then re-precipitation of these phases on the carbon film.

Figure E.18 shows TEM images of partially dissolved material. Various different morphologies can be seen in the images that were obtained at different magnifications. The dissolution was tracked through automated particle analysis and some of the results from this are shown in Figure E.19 and Figure E.20. Ternary diagrams show the loss of sodium-bearing materials from the field of view. However, the distribution scatter plot with Al and particle size shows that the Al particles were relatively unchanged following the dissolution process. The bubble chart plots the sodium nitrate particles with the bubbles representing the size of the particles. Graphically, these plots demonstrate the significant effect of mild dissolution on the sodium phase.

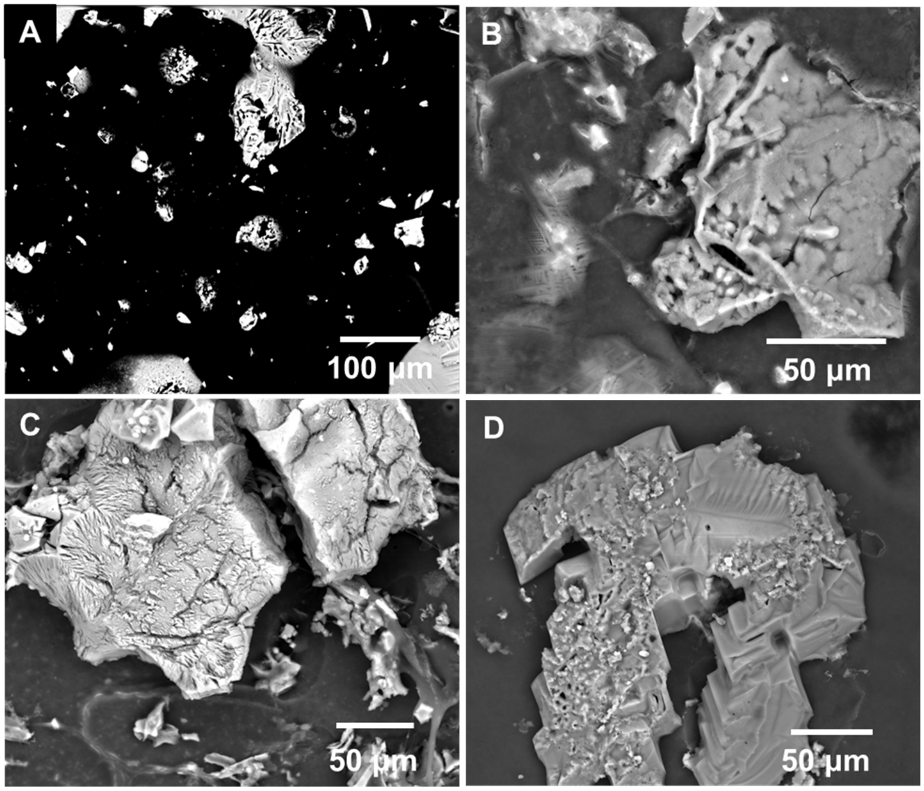

Figure E.18. SEM image of partially dissolved phases showing how the solution has eaten away parts of the crystals: (A) low-magnification view shows hollowed out particles, (B-C) particles with corroded surfaces, and (D) steps are revealed in the dissolution process.

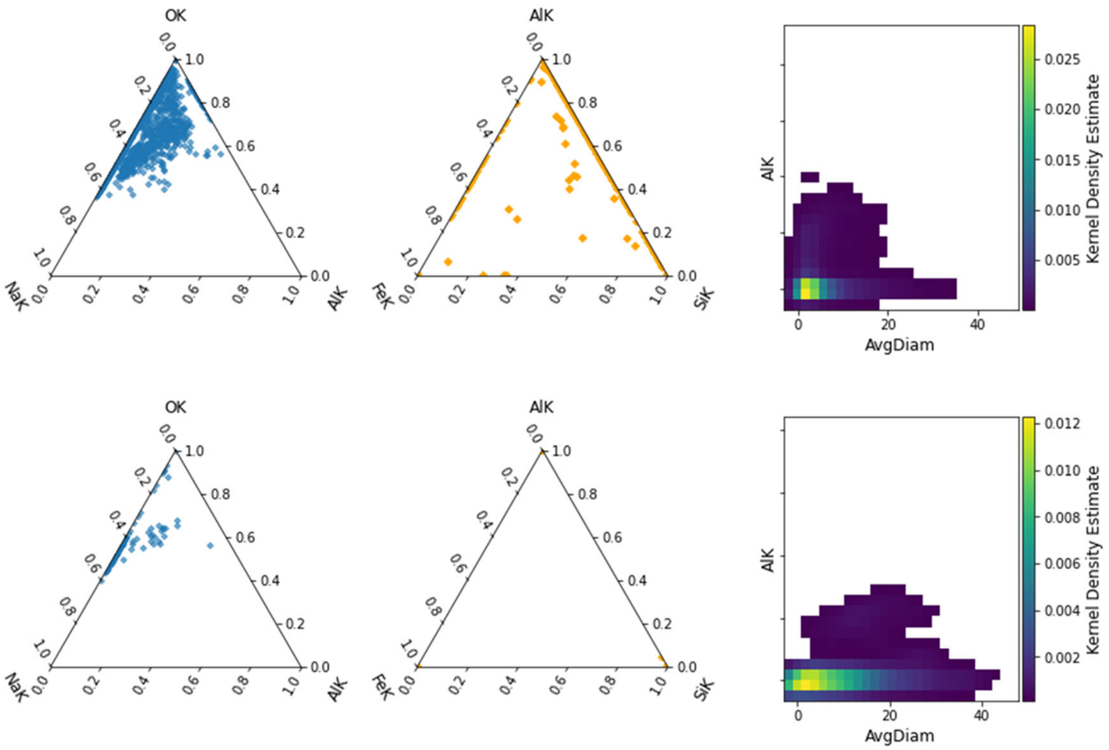

Figure E.19. Effect of dissolution on the particle composition of AP-101 supernatant through ternary phase diagrams and compositional-particle size distributions, showing the loss of sodium-bearing phases.

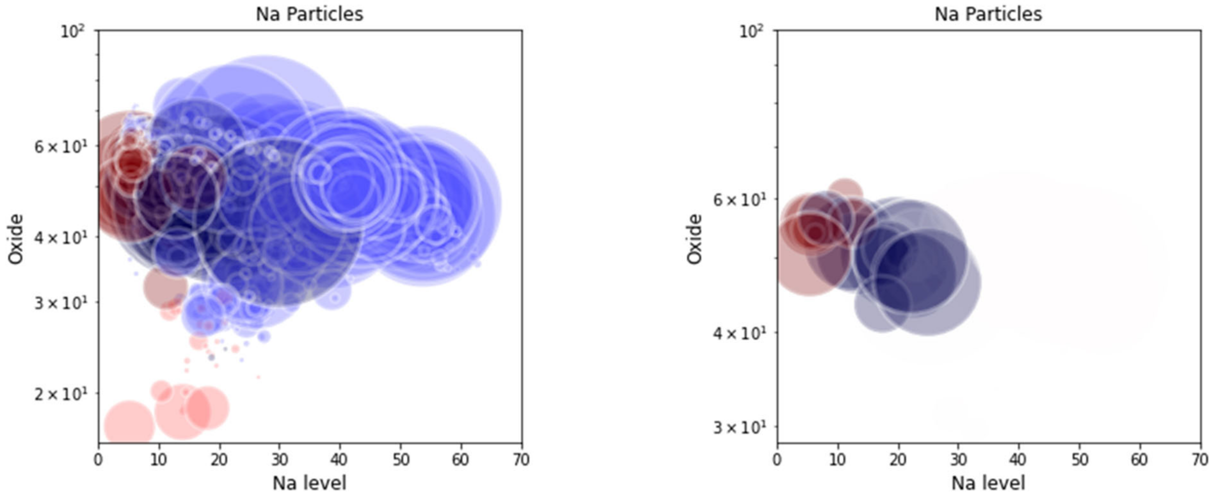

Figure E.20. Bubble plots showing the loss of sodium-bearing phases during dissolution and the change in average particle size.

This experiment demonstrates some of the potential for SEM combined with automated particle analysis to provide more quantitative data on processing operations. The dissolution experiment here was a demonstration of the capabilities of this new tool to describe the dissolution behavior.

E.5 Conclusions of Microscopy Study

Automated particle analysis was used to examine thousands of particles in the SEM and combined with an in-situ corrosion process to demonstrate the impact of simple dissolution of the phase distribution. However, because of the very rapid precipitation of phases, particle size data appeared to be less valid. Particle size depended on how the sample for SEM was prepared. For the solid sample, the material had to be scraped out of the vial and this resulted in a non-representative particle size distribution. When the sample was prepared by filtration from the supernatant, crystals could easily form. The smaller particles, such as the aluminosilicate, do represent particles that were already present and stable in the supernatant prior to any preparation.

E.6 References

Brożek-Mucha Z. 2014. “Scanning electron microscopy and X-ray microanalysis for chemical and morphological characterisation of the inorganic component of gunshot residue: selected problems.” *BioMed Research International* 2014:428038-428038.

Buck EC and BK McNamara. 2004. “Precipitation of nitrate-cancrinite in Hanford tank sludge.” *Environmental Science & Technology* 38(16):4432-4438.

Cantrell KJ, W Um, BD Williams, ME Bowden, B Gartman, WW Lukens, EC Buck, and EJ Mausolf. 2014. “Chemical stabilization of Hanford tank residual waste.” *Journal of Nuclear Materials* 446(1-3):246-256.

Esch RA. 1996. Final Report for Tank 241-AP-101, Grab Samples 1AP-95-1, 1AP-95-2, 1AP-95-3, 1AP-95-4, 1AP-95-5, and 1AP-95-6. WHC-SD-WM-DP-161, Rev. 1. Westinghouse Hanford Co., Richland, Washington.

Fiskum SK, PR Bredt, JA Campbell, OT Farmer, LR Greenwood, EW Hoppe, FV Hoopes, GJ Lumetta, GM Mong, RT Ratner, CZ Soderquist, MJ Steele, RG Swoboda, MW Urie, and JJ Wagner. 2000. *Inorganic, Radioisotopic, and Organic Analysis of 241-AP-101 Tank Waste.* PNNL-13354 (formerly PNWD-3046); WTP-RPT-009, Rev. 0. Prepared for CH2M Hanford Group by Pacific Northwest National Laboratory, Richland, Washington.

Herting DL and GA Cooke. 2002. *Identification of Solid Phases in Saltcake from Hanford Site Waste Tanks*. HNF-1185, Rev. 0; HNF-EDC-02-12376. Fluor Hanford, Richland, Washington.

Krupka KM, HT Schaef, BW Arey, SM Heald, WJ Deutsch, MJ Lindberg, and KJ Cantrell. 2006. “Residual Waste from Hanford Tanks 241-C-203 and 241-C-204. 1. Solids Characterization.” *Environmental Science & Technology* 40(12):3749-3754.

Laskin A and JP Cowin. 2001. “Automated Single-Particle SEM/EDX Analysis of Submicrometer Particles down to 0.1 μm.” *Analytical Chemistry* 73(5):1023-1029.

Lumetta GJ, BK McNamara, EC Buck, SK Fiskum, and LA Snow. 2009. “Characterization of High Phosphate Radioactive Tank Waste and Simulant Development.” *Environmental Science & Technology* 43(20):7843-7848.

Mitchell DRG. 2008. "DiffTools: Electron diffraction software tools for DigitalMicrograph™." *Microscopy Research and Technique* 71(8):588-593.

Wells BE, DE Kurath, LA Mahoney, Y Onishi, JL Huckaby, SK Cooley, CA Burns, EC Buck, J Tingey, and RC Daniel. 2011. *Hanford Waste Physical and Rheological Properties: Data and Gaps*. PNNL-20646. Pacific Northwest National Laboratory, Richland, Washington.

Pacific Northwest
National Laboratory

902 Battelle Boulevard
P.O. Box 999
Richland, WA 99354
1-888-375-PNNL (7665)

www.pnnl.gov